Modified Clp Protease Complex in the ClpP3 Null Mutant and Consequences for Chloroplast Development and Function in Arabidopsis[1][C][W][OA]

Jitae Kim, Paul Dominic Olinares[2], Soo-hyun Oh, Stefania Ghisaura[3], Anton Poliakov[4], Lalit Ponnala, and Klaas J. van Wijk*

Department of Plant Biology (J.K., P.D.O., S.-h.O., S.G., A.P., K.J.v.W.) and Computational Biology Service Unit (L.P.), Cornell University, Ithaca, New York 14853

The plastid ClpPRT protease consists of two heptameric rings of ClpP1/ClpR1/ClpR2/ClpR3/ClpR4 (the R-ring) and ClpP3/ClpP4/ClpP5/ClpP6 (the P-ring) and peripherally associated ClpT1/ClpT2 subunits. Here, we address the contributions of ClpP3 and ClpP4 to ClpPRT core organization and function in Arabidopsis (*Arabidopsis thaliana*). ClpP4 is strictly required for embryogenesis, similar to ClpP5. In contrast, loss of ClpP3 (*clpp3-1*) leads to arrest at the hypocotyl stage; this developmental arrest can be removed by supplementation with sucrose or glucose. Heterotrophically grown *clpp3-1* can be transferred to soil and generate viable seed, which is surprising, since we previously showed that *CLPR2* and *CLPR4* null alleles are always sterile and die on soil. Based on native gels and mass spectrometry-based quantification, we show that despite the loss of ClpP3, modified ClpPR core(s) could be formed, albeit at strongly reduced levels. A large portion of ClpPR subunits accumulated in heptameric rings, with overaccumulation of ClpP1/ClpP5/ClpP6 and ClpR3. Remarkably, the association of ClpT1 to the modified Clp core was unchanged. Large-scale quantitative proteomics assays of *clpp3-1* showed a 50% loss of photosynthetic capacity and the up-regulation of plastoglobules and all chloroplast stromal chaperone systems. Specific chloroplast proteases were significantly up-regulated, whereas the major thylakoid protease (FtsH1/FtsH2/FtsH5/FtsH8) was clearly unchanged, indicating a controlled protease network response. *clpp3-1* showed a systematic decrease of chloroplast-encoded proteins that are part of the photosynthetic apparatus but not of chloroplast-encoded proteins with other functions. Candidate substrates and an explanation for the differential phenotypes between the *CLPP3*, *CLPP4*, and *CLPP5* null mutants are discussed.

Intracellular proteolysis is essential for proteome homeostasis, the regulation of metabolic and signaling pathways, and, ultimately, the maintenance of organellar and cellular viability. Chloroplasts contain multiple soluble and membrane-bound proteases and processing peptidases (Kato and Sakamoto, 2010; Olinares et al., 2011b) that operate in parallel as well as in series, presumably with partially overlapping substrates. The Clp protease system is the most abundant and complex stromal protease family in the plastid. It consists of five Ser-type Clp proteases (P1 and P3–P6) and four nonproteolytic ClpR subunits (R1–R4), which together constitute the tetradecameric and asymmetric approximately 350-kD Clp protease core formed by two heptameric rings. Furthermore, three Clp AAA+ chaperones (C1, C2, and D) similar to the *Escherichia coli* ClpA and the adaptor ClpS (homologous to the *E. coli* ClpS) likely serve to deliver protein substrates to the core complex. Attached to the ClpPR core are ClpT1 and ClpT2, which have similarity to the N-terminal domain of the ClpC/ClpD chaperones (Peltier et al., 2004; Olinares et al., 2011a). These ClpT subunits are unique to chloroplasts and have been hypothesized to regulate chaperone binding and/or substrate selection (Peltier et al., 2004; Olinares et al., 2011b) or to aid in the assembly of the ClpPR core complex (Sjögren and Clarke, 2011).

The quantitative subunit compositions for the intact ClpPR core and each heptameric ring were recently determined (Olinares et al., 2011a). The chloroplast ClpP/ClpR protease was affinity purified from *clpr4* and *clpp3* Arabidopsis (*Arabidopsis thaliana*) null mutants complemented with C-terminal StrepII-tagged versions of CLPR4 and CLPP3, respectively. The subunit stoichiometry was determined by a mass spectrometry

[1] This work was supported by the National Science Foundation (grant no. MCB–1021963 to K.J.v.W.). Part of this work was carried out by using the resources of the Computational Biology Service Unit of Cornell University, which is partially funded by the Microsoft Corporation.

[2] Present address: Laboratory of Mass Spectrometry and Gaseous Ion Chemistry, The Rockefeller University, New York, NY 10065.

[3] Present address: Porto Conte Ricerche, Tramariglio, Alghero (Sassari), Italy.

[4] Present address: Department of Pathology, University of Michigan, Ann Arbor, MI 48109.

* Corresponding author; e-mail kv35@cornell.edu.

The author responsible for distribution of materials integral to the findings presented in this article in accordance with the policy described in the Instructions for Authors (www.plantphysiol.org) is: Klaas J. van Wijk (kv35@cornell.edu).

[C] Some figures in this article are displayed in color online but in black and white in the print edition.

[W] The online version of this article contains Web-only data.

[OA] Open Access articles can be viewed online without a subscription.

www.plantphysiol.org/cgi/doi/10.1104/pp.113.215699

(MS)-based multiplexed absolute quantification strategy using a concatamer of stable isotope-labeled proteotypic peptides generated from a synthetic gene, also known as the QconCAT approach (Beynon et al., 2005; Pratt et al., 2006). This showed that the ClpPR core consisted of one heptameric ring containing ClpP3, ClpP4, ClpP5, and ClpP6 in a 1:2:3:1 ratio (designated the P-ring) and the other ring containing ClpP1 and ClpR1, ClpR2, ClpR3, and ClpR4 in a 3:1:1:1:1 ratio (designated the R-ring). Moreover, based on biochemical and phylogenetic analysis, it was suggested that ClpT1 and ClpT2 bind to the adaxial side of the P-ring (Olinares et al., 2011a; Sjögren and Clarke, 2011). This Clp core complexity is puzzling and is very different from the much simpler Clp composition in photosynthetic and nonphotosynthetic bacteria. The complexity of the plastid Clp core contrasts also to the homomeric ClpP2 core in plant mitochondria (Peltier et al., 2004) and is specific to higher plants and green algae (Derrien et al., 2012). This suggests a specific adaptation of the ClpPRT protease to the chloroplast proteome, warranting an in-depth analysis.

Genetic and phenotypic analyses of various *CLPPR* mutants in Arabidopsis showed that each of the tested genes affects embryogenesis or seedling development and chloroplast biogenesis. Interestingly, the severity of the phenotypes for the various *CLPPR* null mutants differs greatly (for review, see Olinares et al., 2011b). Complete loss of *CLPP5* gene expression is embryo lethal, whereas complete loss of *CLPR2* or *CLPR4* delayed embryogenesis and resulted in developmental arrest at the cotyledon stage (Kim et al., 2009). This arrest could be broken by growth on Suc, but seedlings remained sterile (Kim et al., 2009; Olinares et al., 2011b). The *Arabidopsis clpr1-1* null mutant could be maintained on soil and produced viable seeds, even if they showed a virescent phenotype (Koussevitzky et al., 2007). Overexpression of *CLPR3*, but not *CLPR2* or *CLPR4*, in *clpr1-1* led to full complementation, indicating that ClpR1 is partially redundant to ClpR3 (Kim et al., 2009). In addition, ClpP1, the only plastid-encoded Clp subunit, was shown to be essential for leaf development in tobacco (*Nicotiana tabacum*; Shikanai et al., 2001; Kuroda and Maliga, 2003). A mutant in *CLPR2* with approximately 20% residual *CLPR2* mRNA and ClpR2 protein (*clpr2-1*; Rudella et al., 2006) and antisense lines against *CLPP4* and *CLPP6* (Sjögren et al., 2006; Zheng et al., 2006) in Arabidopsis exhibited delayed chloroplast and plant development and a virescent or variegated phenotype.

It is not known if *CLPP3*, *CLPP4*, or *CLPP6* is essential for embryogenesis, similar to *CLPP5*. One of the objectives of this study was to address the structural and functional contributions of ClpP3 and ClpP4 and, thus, to complete the genetic analysis of the ClpPR core subunits in Arabidopsis; we note that there are no suitable transferred DNA (T-DNA) insertion mutants for *CLPR3* or *CLPP6*. We will show that null mutants for *CLPP4* are embryo lethal, similar to *CLPP5*, but that null mutants for *CLPP3* can germinate, develop seedlings under heterotrophic but not autotrophic conditions, and even produce viable seeds. Thus, in contrast to *CLPP4* and *CLPP5* null mutants, *clpp3-1* is the only null mutant in a ClpP protease subunit that can germinate, likely because other ClpPR subunits can partially substitute for ClpP3. Using the QconCAT technique (Olinares et al., 2011a), we also determined the composition of the ClpPR core in *clpp3-1* in an effort to understand how the Clp system can function (even if suboptimally) without ClpP3. Furthermore, we quantified ClpT1/ClpT2 in the various Clp assemblies using immunodetection. Previously, we determined the leaf proteome phenotypes of *clpr2-1* (Zybailov et al., 2009a) and *clpr4-1* (Kim et al., 2009) using MS-based spectral counting methodology. These studies identified approximately 2,800 proteins, and quantification revealed that the strongest effects occurred within the chloroplast, which is consistent with their yellow/pale-green phenotype and delayed growth. A strong loss of the photosynthetic machinery was observed in the leaf proteome of *clpr4-1*, consistent with its severe albino phenotype and its dependence on exogenous sugar (Kim et al., 2009). Here, we further optimized this large-scale proteomics workflow and developed and implemented a better statistical analysis to determine the molecular phenotype of *clpp3-1*. Comparison of the proteomics phenotype of *clpp3-1* with the *clpr2-1* and *clpr4-1* phenotypes indicated very similar metabolic and protein homeostasis defects for these Clp core mutants.

RESULTS

ClpP4 Is Essential for Embryogenesis

We screened and genotyped various T-DNA insertion collections with the Columbia-0 background for potential null and knockdown mutants in *CLPP4* (AT5g45390). This identified one null mutant line (SALK_000913), designated *clpp4-1* (Fig. 1A). Developing seeds in siliques of heterozygous plants showed a 3:1 green:white ratio and no abortions, whereas mature siliques showed smaller, darker seeds in the same ratio (Fig. 1B). This is consistent with a single genome insertion in a gene important for plastid development and/or function. None of the progeny of such heterozygous *clpp4-1* mutants survived as homozygotes, even when grown under heterotrophic conditions and at low light intensities. Microscopy showed a block in embryogenesis at the (pre)globular stage in the white seeds (Fig. 1C). Heterozygous *clpp4-1* had a wild-type phenotype, indicative of recessive alleles without a gene dosage effect (data not shown). *clpp4-1* null alleles were recovered in lines transformed with *CLPP4* complementary DNA (cDNA) driven by a 1× 35S promoter, and reverse transcription (RT)-PCR confirmed complementation, further showing that loss of *CLPP4* is responsible for the embryo-lethal phenotype (Fig. 1D). Thus, ClpP4 is essential for embryogenesis similar to ClpP5 but unlike the other nucleus-encoded chloroplast Clp core proteins for which null mutants have been tested so far (*CLPR1*, *CLPR2*, and *CLPR4*; Kim et al., 2009).

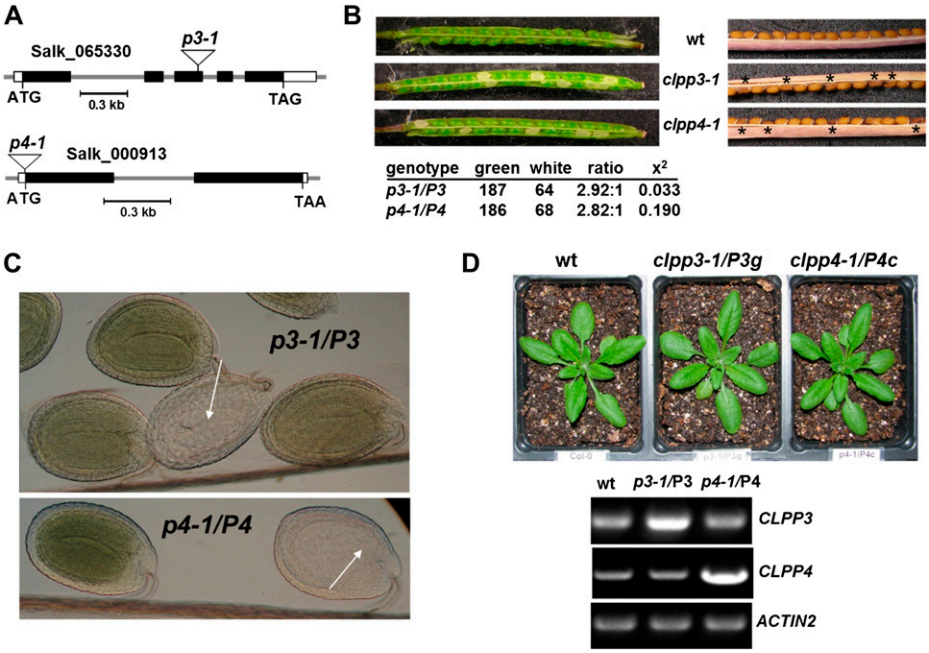

Figure 1. Genotyping and embryo phenotypes in the CLPP3 and CLPP4 mutants. A, Gene model structures and positions of T-DNA insertions in the CLPP3 and CLPP4 null mutants (*clpp3-1* and *clpp4-1*, respectively) used in this study. Exons (black boxes for coding sequence), 5′ and 3′ untranslated regions (white boxes), and T-DNA insertions (triangles) are indicated. B, Segregation analysis of green and white seeds in developing and mature siliques of heterozygous *clpp3-1* and *clpp4-1*. Asterisks mark smaller and darker colored seeds, likely representing homozygous mutants. wt, Wild type. C, Nomarski bright-field microscopy of cleared seeds of siliques of heterozygous *clpp3-1* and *clp4-1*. Arrows indicate the underdeveloped embryos in the colorless seeds (torpedo stage in *clpp3-1* and [pre]globular stage for *clpp4-1*). D, Complementation of *clpp3-1* (*clpp3-1/P3g*) and *clpp4-1* (*clp4-1/P4c*) using *CLPP3* genomic DNA and *CLPP4* cDNA, respectively. Complementation was confirmed at the mRNA level by RT-PCR.

Loss of ClpP3 Results in Delayed Embryo Development and Seedling Lethality But Can Be Rescued by Adding Sugars to the Growth Medium

We also screened T-DNA insertion collections with the Columbia-0 background for potential null and knockdown mutants in *CLPP3* (AT1G66670). This identified one null mutant line (SALK_065330), designated *clpp3-1* (Fig. 1A). Similar to *clpp4-1*, the developing seeds in siliques of heterozygous *clpp3-1* plants showed a 3:1 green: white ratio and no abortions, again consistent with a single insertion (Fig. 1B). Microscopy showed delayed embryogenesis, mostly reaching the torpedo stage in the white seeds (Fig. 1C). The homozygous *clpp3-1* could be fully complemented with genomic *CLPP3* (Fig. 1D) and to a lesser extent also with 1×35S-cDNA-*CLPP3-StrepII* (Olinares et al., 2011a). PCR of genomic DNA (data not shown) and RT-PCR (Fig. 1D) confirmed the complementation.

Under autotrophic conditions on agar plates, homozygous *clpp3-1* seedlings were identified, but their development was arrested at the cotyledon stage and seedlings died after several weeks (Fig. 2A), similar to null mutants in *CLPR2* and *CLPR4* (Kim et al., 2009). We note that the hypocotyls of *clpp3-1* seedlings were clearly greener than *clpr2-2* and *clpr4-1* null alleles (Fig. 2A). Under heterotrophic conditions on agar plates supplemented with 1% to 2% Suc, homozygous *clpp3-1* seedlings developed beyond the cotyledon stage, even if growth and development were slow, and with pale-green serrated leaves (Fig. 2B), as observed previously for *CLPR2* and *CLPR4* null alleles. The *clpp3-1* allele accumulated neither *CLPP3* mRNA nor ClpP3 protein (Fig. 2C). *clpp3-1* plants grown on agar were greener on 2% Suc than on 1% Suc, and the youngest leaves were paler than the older leaves (Fig. 2D). The chlorophyll and carotenoid concentrations in *clpp3-1*, on a fresh weight basis, of 7-week-old seedlings grown on agar medium supplemented with 2% Suc were reduced by 77% and 65%, respectively, compared with the wild type (Supplemental Table S1). The total chlorophyll-total carotenoid ratio in *clpp3-1* was reduced by 33%.

In many plant studies, Glc is considered primarily a signaling molecule, whereas Suc is primarily considered a source of energy (and used for long-distance transport; Hanson and Smeekens, 2009; Eveland and Jackson, 2012). Therefore, we compared the effects of Suc (1%, 3%, and 5%) and Glc (1%, 3%, and 5%) on seedling development in *clpp3-1*. For comparison, we also included the leaky *clpr2-1* allele, which does not show seedling arrest but has strongly delayed development; this is the Clp core mutant with the strongest

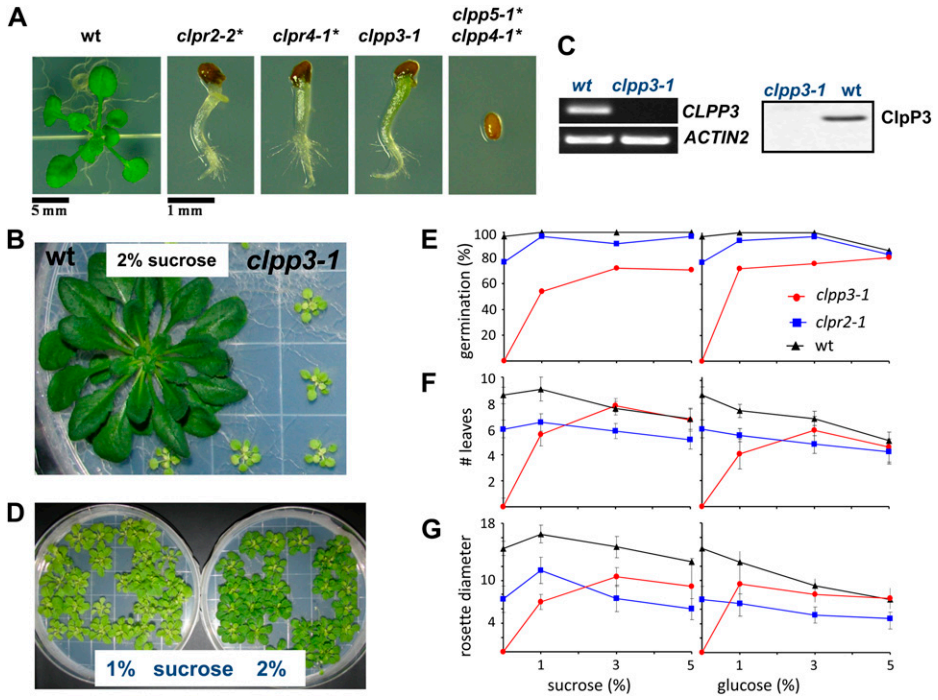

Figure 2. Development of *clpp3-1* on agar plates with or without sugars. A, Development of wild-type (wt) and homozygous *clpp3-1* and *clpp4-1* plants on agar plates with one-half-strength Murashige and Skoog medium without Suc grown under a 10-h/14-h light/dark cycle at 40 μmol photons m^{-2} s^{-1}. Plants are 4 weeks old. For comparison, seedlings from the null mutant lines *clpr2-2* and *clpr4-1* are also shown. *Additional independent null alleles for *CLPR2* and *CLPR4* showed identical phenotypes (Kim et al., 2009). Homozygous seeds for the null mutant lines *clpp4-1* and *clpp5-1* (nor for additional independent alleles for both genes indicated by the asterisks) never germinated. B, Comparison of wild-type and homozygous *clpp3-1* plants on agar plates with one-half-strength Murashige and Skoog medium and 2% Suc grown under a 10-h/14-h light/dark cycle at 40 μmol photons m^{-2} s^{-1}. Plants are 9 weeks old. C, mRNA levels of *CLPP3* and the *ACTIN2* control in the wild type and *clpp3-1* by RT-PCR (left panel). ClpP3 protein levels in the wild type and *clpp3-1* are shown in the right panel with equal amounts (15 μg) of total leaf proteins loaded in each lane on the SDS-PAGE gel. D, Comparison of homozygous *clpp3-1* plants on agar plates with one-half-strength Murashige and Skoog medium with 1% or 2% Suc grown under a 10-h/14-h light/dark cycle at 40 μmol photons m^{-2} s^{-1}. Plants are 13 weeks old. E, Effect of Suc (1%–5%) and Glc (1%–5%) in the wild type, *clpr2-1*, and *clpp3-1* on germination rate ($n = 44$), number of leaves ($n = 12$), and rosette diameter ($n = 10$) measured after 28 d of sowing. SD values are indicated.

phenotype that can still produce seeds (Rudella et al., 2006). Both Suc (1%–5%) and Glc (1%–5%) broke *clpp3-1* seedling arrest for up to 80%, with Glc being somewhat more effective (Fig. 2E). Both sugars strongly stimulated leaf development of *clpp3-1* seedlings, as measured by the number of leaves, with an optimum concentration of 3% for both sugars, but leaf formation was faster on Suc (Fig. 2F). In the wild type and *clpr2-1*, both sugars repressed leaf formation at the higher concentrations (3% and 5%). Glc and Suc showed differential effects on leaf expansion of the wild type, *clpp3-1*, and *clpr2-1*, as measured by the rosette diameter (Fig. 2G). For all three genotypes, Suc stimulated rosette diameter, with the largest diameter at 1% Suc for the wild type (16 cm) and *clpr2-1* (11 cm) but at 3% Suc for *clpp3-1* (10 cm). Rosette diameter was repressed at 3% and 5% Suc for the wild type and *clpr2-1*. In contrast, Glc showed a concentration-dependent repression of rosette diameter for the wild type and *clpr2-1*. In the case of *clpp3-1*, 1% Glc facilitated seedling development by breaking developmental arrest, but higher concentrations repressed leaf growth and expansion, similar to the wild type and *clpr2*. Increased concentrations of Glc, but not Suc, slightly increased chlorophyll and total carotenoid levels on a fresh weight basis in *clpp3-1*. Increase of either Glc or Suc levels increased pigment levels on a fresh weight basis in the wild type and *clpr2-1*, presumably by reduced cell expansion and unaffected pigment accumulation (Supplemental Fig. S1).

The *clpp3-1* Null Allele Can Flower and Produce Viable Seeds, Unlike the Other Seedling-Lethal ClpPR Core Mutants

After several weeks on Suc, *clpp3-1* seedlings started to green and accumulate chlorophyll, and surprisingly, they could be transferred to soil, eventually flowered, and generated viable seeds (Fig. 3), unlike the *CLPR2* and *CLPR4* null alleles, which died soon after transfer

to soil (Kim et al., 2009). Chlorophyll and carotenoid levels of these *clpp3-1* plants were about 50% lower than in wild-type plants (Supplemental Table S1). Thus, *CLPP3* is different from *CLPR2*, *CLPR4*, *CLPP4*, and *CLPP5*, indicating that *CLPP3* is not strictly essential once chloroplasts and leaves have reached the mature stage. This suggested that other CLP-P/CLP-R subunits partially compensate for the loss of ClpP3 (even if very poorly and only late in development). Because in wild-type Columbia-0 plants, ClpP3 is only found in the P-ring with other nucleus-encoded ClpP subunits (ClpP4–ClpP6), it seemed most logical that these nucleus-encoded ClpP subunits substitute for ClpP3. This would be similar to the replacement of ClpR1 by ClpR3 in the R-ring, as we showed previously through overexpression of *CLPR3* cDNA in the *clpr1-1* background (Kim et al., 2009). Therefore, we tested if overexpression of *CLPP4*, *CLPP5*, or *CLPP6* could complement the *clpp3-1* mutants. *clpp3-1* heterozygous plants were transformed with *CLPP4*, *CLPP5*, or *CLPP6* cDNAs using both 2×35S promoters (pMDC32 binary vector) and 1×35S promoters (pEARLYGATE100) and the cDNA for *CLPP3* as a positive control. Numerous complemented *clpp3-1* lines with *CLPP3* StrepII-tag cDNA were recovered, in addition to complemented lines with genomic DNA (Fig. 1D). Despite these extensive efforts, no complementation was observed for overexpression with *CLPP4*, *CLPP5*, or *CLPP6*. This suggests that these nucleus-encoded ClpP proteins by themselves cannot functionally substitute for ClpP3, but overexpression of multiple CLPPs together might be able to complement *clpp3-1*, as our biochemical analysis of Clp complexes in *clpp3-1* seems to suggest (see below).

Synergistic Genetic Interactions between CLPP3 and CLPR2

To explore the relationship between the P- and R-rings of the ClpPR core complex, we investigated the genetic interaction between *clpp3-1* and *clpr2-1*. The double homozygous *clpp3-1* × *clpr2-1* mutant was recovered from plants grown under heterotrophic conditions at low light (Fig. 4A) but was not viable when transferred to soil. This double mutant was extremely reduced in growth and development and remained yellow to very pale green and never produced flowers, even under the most favorable conditions (i.e. low light and 1%–2% Suc). Thus, *clpp3-1* and *clpr2-1* have a synergistic effect.

Interestingly, we observed a clear gene dosage effect of *CLPP3* (heterozygote) on the homozygous *clpr2-1* mutant. The double mutant homozygous for the *clpr2-1* allele but heterozygous for the *clpp3-1* allele (Aabb) is shown in Figure 4B. This double mutant has a stronger phenotype than *clpr2-1* but can be still grown on soil and produces viable seeds. The double mutant homozygous for the *clpp3-1* allele but heterozygous for the *clpr2-1* allele (aaBb) has the same phenotype as the *clpp3-1* single mutant (data not shown). RT-PCR confirmed the reduced mRNA for *CLPR2* in the *clpr2-1* background and complete loss for *CLPP3* in the double homozygous mutant. A partial reduction for *CLPP3* was observed in heterozygous *clpp3-1* in the homozygous *clpr2-1* background (Fig. 4C). Furthermore, *CLPR2* mRNA levels were influenced by the levels of *CLPP3* mRNA. It can thus be concluded that there is an interaction effect between the expression/accumulation of subunits of the P- and R-rings, similar to subunits within the R-ring (when crossing ClpR1 and ClpR2 alleles; Kim et al., 2009).

Accumulation and Assembly State of ClpPRT Subunits in *clpp3-1*

To determine if other Clp subunits are up-regulated to compensate for the loss of ClpP3, or otherwise affected, we determined accumulation levels for the ClpPR core proteins ClpR2, ClpP3, ClpP4, and ClpP6, peripheral subunits ClpT1 and ClpT2, the substrate regulator ClpS, and the Clp chaperones ClpC1 and ClpC2 using immunoblotting. Total leaf proteins were extracted from *clpp3-1* plants transferred to soil as well as wild-type plants at a comparable developmental stage. SDS-PAGE followed by immunoblotting showed that the accumulation level of ClpR2 was unchanged in the *clpp3-1* mutant, whereas accumulation levels of ClpP4, ClpP6, ClpT1, and ClpT2 were 2- to 3-fold up-regulated in *clpp3-1* (Fig. 5). The ClpS level increased 4-fold in *clpp3-1*. Moreover, ClpC1 and ClpC2 were both down-regulated by 30%. Interestingly, in *clpp3-1*, most of ClpT1, but not ClpT2, showed an approximately 1-kD upward mass

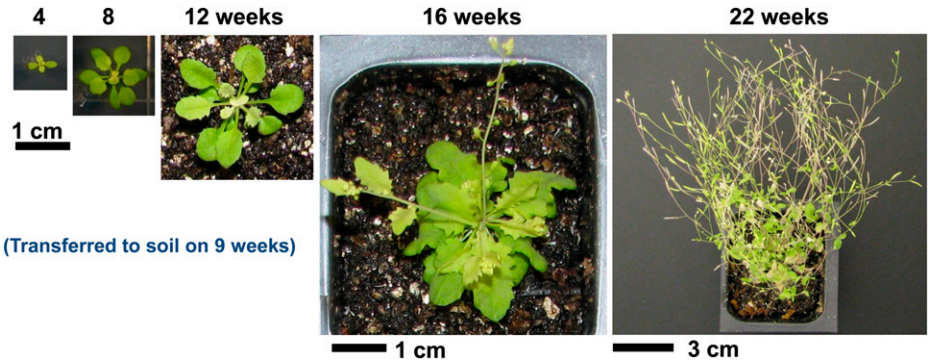

Figure 3. *clpp3-1* can flower and produce viable seed. The development series shows *clpp3-1* first grown on agar plates with one-half-strength Murashige and Skoog medium and 2% Suc under a 10-h/14-h light/dark cycle at 40 μmol photons m^{-2} s^{-1} for 9 weeks and then transferred to soil and grown under a 16-h/8-h light/dark cycle at 120 μmol photons m^{-2} s^{-1}.

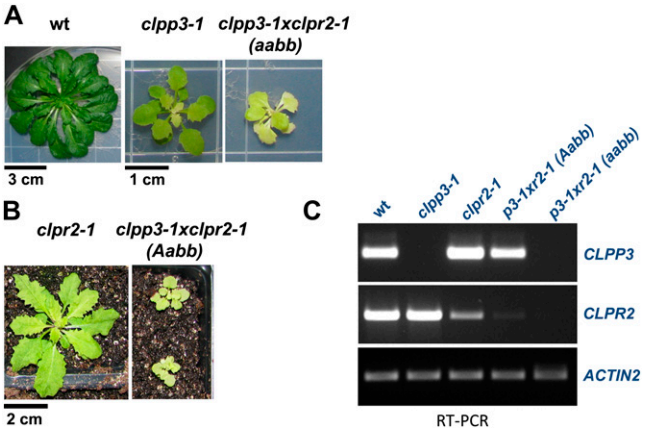

Figure 4. The genetic interaction of *clpp3-1* with *clpr2-1* indicates a synergistic effect between the alleles. A, The double homozygous mutant *clpp3-1*×*clpr2-1* (right panel) was grown on agar plates with one-half-strength Murashige and Skoog medium and 2% Suc under a 10-h/14-h light/dark cycle at 40 μmol photons m^{-2} s^{-1} for 75 d. The double mutant never flowered and was not viable when transferred to soil. For comparison, wild-type (wt) and parent *clpp3-1* plants are shown in the left and middle panels. B, Dosage effect of the *clpp3-1* allele in the *clpr2-1* background. Seedlings, homozygous for *clpr2-1* but heterozygous for *clpp3-1* (right panel), were grown on soil for 7 weeks under an 18-h/6-h light/dark cycle at 100 μmol photons m^{-2} s^{-1}. For comparison, parent *clpr2-1* is shown in the left panel grown together with the double mutant. C, *CLPP3* and *CLPR2* mRNA accumulation for the wild type, *clpr2-1*, *clpp3-1*, and the *clpp3-1*×*clpr2-1* double mutant and *ACTIN2* as a control, using RT-PCR.

shift due to an unknown posttranslational modification or modified processing (Fig. 5).

To determine the consequences of the loss of ClpP3 on the assembly state of the ClpPR complex and the association of ClpT, chloroplast soluble proteomes (stroma) of the wild type and *clpp3-1* were extracted under nondenaturing conditions, and proteins were separated by one-dimensional native gel electrophoresis. For comparison, we also included the *clpr2-1* mutant in the analysis. In the wild type, ClpR2, ClpP4, and ClpP6 were mostly observed in the expected 350-kD tetradecameric ClpPRT complex (Fig. 6). However, some signal (in particular for ClpR2) was also detected in a band around 200 kD, corresponding with single heptameric rings; this reflects destabilization of the tetradecamer at the heptamer interface, similar to our previous observations (Olinares et al., 2011a; Fig. 6). In the case of *clpr2-1*, the total signal for ClpR2 was reduced, which is consistent with the 5-fold reduced expression in *clpr2-1* reported previously (Rudella et al., 2006). Similar to the wild type, ClpR2 in *clpr2-1* was mostly found in the 350-kD complex, with lower amounts accumulating in the 200-kD heptamers. In contrast, in *clpp3-1*, nearly all of ClpR2 and ClpP4 were found around 200 kD, with only small amounts accumulating between 350 and 400 kD. It also appears that this complex was about 50 kD larger than the 350-kD band observed in the wild type and *clpr2-1*. ClpP4, but not ClpR2, was found in two bands in the 200-kD region. For both *clpr2-1* and *clpp3-1*, about 50% of ClpP6 accumulated in 350-kD complexes, with the remainder of ClpP6 found in two separate bands in the 200-kD region. In the case of ClpT1, essentially all protein was found in the 350-kD complex for the wild type, *clpr2-1*, and *clpp3-1*. A very small amount (less than 5%) of ClpT1 was also found in a single band around 200 kD in the case of *clpr2-1* and *clpp3-1*. The signals for ClpT2 in the 200- to 400-kD region were very weak and therefore inconclusive, perhaps because the vast majority of ClpT2 accumulated as free monomers or dimers (data not shown).

Together, these results show that in the wild type, a single ClpPRT complex accumulates as expected, with some destabilization occurring, resulting in an accumulation of approximately 200-kD heptameric rings. Previously, we showed by affinity tagging and MS analysis that these heptameric rings contained either ClpP1, ClpR1, ClpR2, ClpR3, and ClpR4 or ClpP3, ClpP4, ClpP5, and ClpP6 (Olinares et al., 2011a). In the case of *clpp3-1*, only ClpP6 and ClpT1, but not ClpP4 and ClpR2, accumulated at high levels in 350- to 400-kD Clp core complexes. In *clpp3-1* and *clpr2-1*, ClpP4 and ClpP6 were found in two complexes in the 200-kD region. The nature of this heterogeneity in the 200-kD region is not clear.

Stoichiometry Determination of Clp Assemblies in *clpp3-1*

To further determine the composition and assembly state of the ClpPR complex in *clpp3-1*, and possibly to

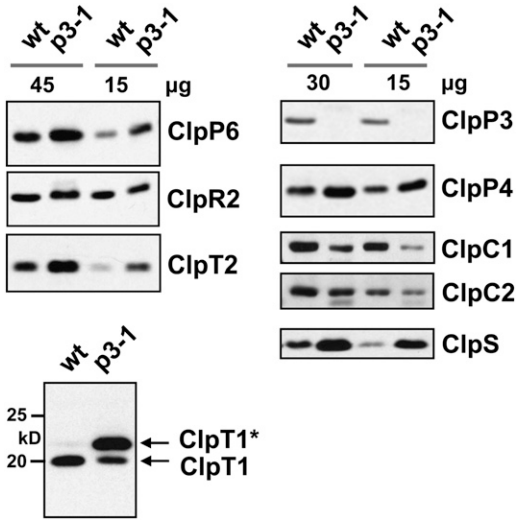

Figure 5. Accumulation levels of Clp proteins in *clpp3-1* as compared with the wild type (wt). Total soluble leaf proteins were extracted from *clpp3-1* and the wild type. *clpp3-1* plants were transferred to soil after initial growth on agar plates with one-half-strength Murashige and Skoog medium supplemented with 2% Suc. Soil-grown wild-type plants were at the same developmental stage. After SDS-PAGE, proteins were transferred to blots and probed with specific antisera against ClpP3, ClpP4, ClpP6, ClpR2, ClpT1, ClpT2, ClpC1, ClpC2, and ClpS. ClpT* indicates ClpT with approximately 1-kD increased mass; this is due to an unknown posttranslational modification or modified processing. The amount of protein loaded in each lane is indicated.

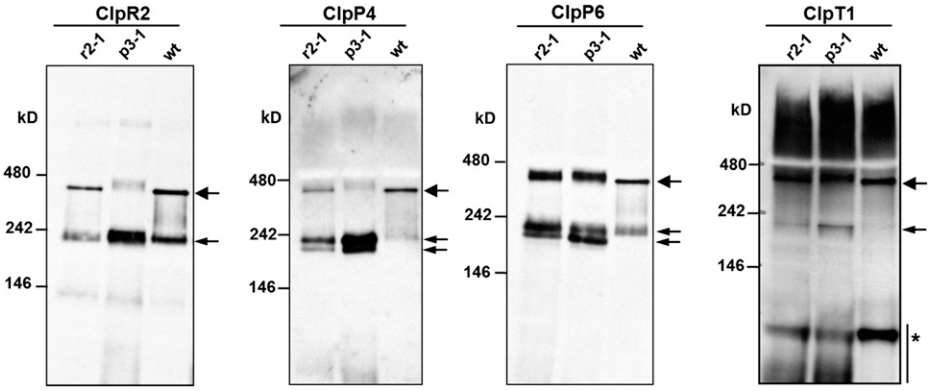

Figure 6. Assembly state of the ClpPRT proteins determined by immunoblot analysis after native gel electrophoresis. Stromal proteins obtained from isolated chloroplasts from the wild type (wt), *clpr2-1*, and *clpp3-1* were separated on native gels, transferred to blots, and probed with antisera against ClpR2, ClpP4, ClpP6, and ClpT1. The larger arrows indicate ClpPRT core complexes (350–400 kD), while the smaller arrows indicate Clp complexes between 180 and 240 kD, corresponding to heptameric ClpPR rings. The lower mass bands on the ClpT1 blot marked with an asterisk are unspecific. Thirty micrograms of stromal protein was loaded in each lane.

determine if one or more Clp subunits compensate for ClpP3 in the assembled core, we implemented the QconCAT approach on chloroplast stroma, but now without StrepII-affinity purification of the Clp assemblies (Fig. 7). This is more challenging because of the higher complexity of the samples, but it was not practically feasible to create such StrepII-tagged Clp lines in the *clpp3-1* background. Chloroplast stromal samples from the wild type and *clpp3-1* were separated by native gel electrophoresis, and the region between 150 and 400 kD was cut into four gel slices, such that it would capture the intact ClpPRT cores (250- to 400-kD range) and the individual heptameric rings (150- to 250-kD range; Fig. 7). Proteins in each gel slice were digested with trypsin, and the resulting peptide mixtures were spiked with the in-gel-digested stable isotope-labeled Clp-QconCAT standard followed by liquid chromatography (LC)-MS analysis using an LTQ-Orbitrap. The absolute amount of each Clp subunit was determined from the measured sample-to-standard peak area ratios of the representative peptides. The MS analysis was carried out in triplicate. This workflow is summarized in Figure 7.

ClpP5, ClpP6, ClpR2, and ClpR4 could be quantified by two distinct peptides each, whereas the amounts of

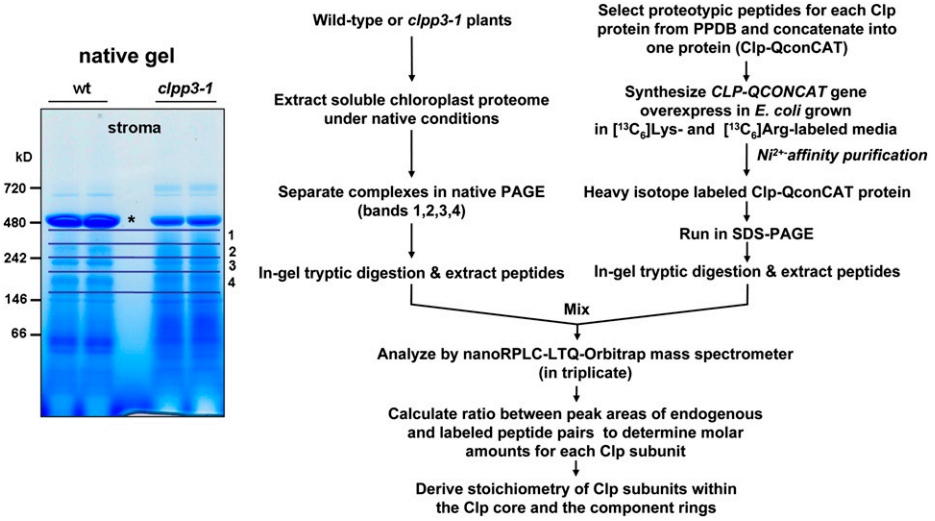

Figure 7. Workflow for determination of the assembly state of the ClpPR proteins in *clpp3-1* and the wild type (wt) by QConCAT analysis. The workflow shown is for the determination of molar amounts of each Clp subunit in different Clp complexes using MS-based quantification using stable isotope-labeled proteotypic peptides generated from a synthetic gene in *E. coli*. Stromal proteomes from *clpp3-1* and the wild type (100 μg per lane in duplicate) were separated on a native gel and stained with Coomassie blue. Bands 1 (350–450 kD), 2 (250–350 kD), 3 (200–250 kD), and 4 (150–200 kD) were cut out, and duplicate bands were pooled and analyzed together. The asterisk indicates the 550-kD Rubisco holocomplex. PPDB, Plant Proteome Database. [See online article for color version of this figure.]

ClpP1, ClpR1, and ClpR3 could be measured by one peptide each (Supplemental Table S2). ClpP4 could not be quantified, since the standard peptides could not be detected due to the relatively high sample complexity. However, we detected ClpP4 from large-scale proteomic analyses of total leaf extracts from *clpp3-1* (see below), and we determined accumulation levels and assembly state from immunoblotting (Figs. 5 and 6); this allowed us to consider ClpP4 as a candidate for compensation of the loss of ClpP3 (see "Discussion"). From the molar amount of each Clp subunit per gel band, the relative distribution of the Clp subunits across various assembly states could be determined (Fig. 8). To simplify the calculations and outcomes, and because the stoichiometries between the Clp subunits were similar between the two gel slices within the 250- to 400-kD range (bands 1 and 2; the Clp core complexes) and also within the 150- to 250-kD range (bands 3 and 4; the heptameric rings), we pooled the data within each of these mass ranges (Supplemental Table S2). Figure 8, A and B, shows the molar distribution of the Clp subunits across the Clp cores and P- and R-rings, whereas Figure 8C shows the overall distribution.

In the wild type, 54% of the Clp subunits were detected in the Clp core complex, with the remaining 46% accumulating in heptamers. In contrast, in *clpp3-1*, only 12% of ClpPR subunits assembled in the Clp cores, with the remaining 88% in Clp heptameric rings (150–250 kD). This indicates that Clp subunits in *clpp3-1* could still associate into Clp rings, but Clp core assembly formation was inefficient, in agreement with the immunoblotting results (Fig. 6).

The asymmetric Clp core complex is composed of the P-ring and the R-ring in a 1:1 stoichiometry and an overall ClpPR stoichiometry for [P3:P4:P5:P6]:[P1:R1:R2:R3:R4] of [1:2:3:1]:[3:1:1:1:1] (Olinares et al., 2011a). To evaluate the stoichiometry of ClpPR proteins in the Clp core complex, we chose ClpR4 as a normalizer, because it could be reliably quantified with two peptides (for details and SD values, see Supplemental Table S2). For the Clp core complex in wild-type stroma (250–450 kD), the molar ratio for [P3:P5:P6]:[P1:R1:R2:R3:R4] was [1:3:1]:[3:1:1:1:1] (Table I), which was identical to what we observed with the affinity-purified Clp core (Olinares et al., 2011a), except that we could not quantify ClpP4. Moreover, the ClpPR stoichiometries in the mixture of individual heptameric rings (between 150 and 250 kD) in the wild type was similar in the core (Table I). In contrast, the ClpPR stoichiometries in the Clp core of *clpp3-1* were altered with increased numbers of ClpP5, ClpP1, and ClpR3 (and complete loss of ClpP3), resulting in an approximate ratio of [0:4:1]:[5:1:1:2:1] for [P3:P5:P6]:[P1:R1:R2:R3:R4], which suggest mixing of the subunits of the R- and P-rings. Similarly, also in the mixture of individual heptameric rings (between 150 and 250 kD), the ratio was changed, now with even stronger overrepresentation of ClpP5 (Table I). Summation of the data for the core and the rings resulted in the expected stoichiometry for the wild type but increased copy numbers for ClpP5, ClpP1, ClpR3, and to a lesser degree ClpP6 for *clpp3-1* (Fig. 8C; Table I). Absolute amounts of ClpR1, ClpR2, and ClpR4 (normalized to total stromal proteins) were unchanged in *clpp3-1* as compared with the wild type, whereas there was 2- to 2.5-fold more ClpP1, ClpP5, ClpP6, and ClpR3 (Fig. 8C).

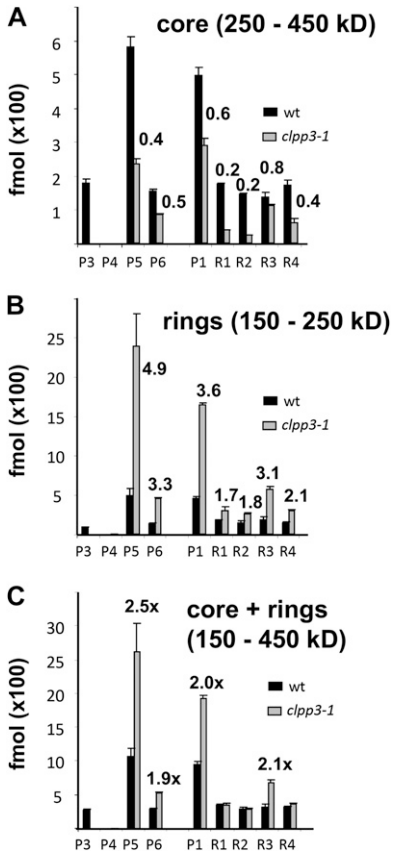

Figure 8. Distribution of Clp subunits among the high-molecular-mass Clp assemblies for the wild type (wt) and *clpp3-1*. The molar amounts of each Clp subunit across mass ranges 250 to 450 kD and 150 to 250 kD were determined using the QconCAT approach as outlined in Figure 7. Subunits were grouped as components of the P-ring (ClpP3, ClpP4, ClpP5, and ClpP6) and the R-ring (ClpP1, ClpR2, ClpR3, and ClpR4). ClpP4 could not be quantified. Absolute amounts of ClpPR subunits (in fmol) in the mass range 250 to 450 kD corresponding to ClpPR core complexes (A), in the mass range 150 to 250 kD corresponding to heptameric rings (B), in the combined samples (across 150 to 450 kD; C) are shown. Values above the bars indicate the *clpp3-1*/wild-type ratio for each protein. SD values are indicated.

Phenotypic Analysis of *clpp3-1* by Comparative Quantitative Proteomics

To gain insight into the consequences of the loss of *CLPP3*, we compared the total denatured leaf proteomes of *clpp3-1* and wild-type rosettes (Fig. 9). Leaf rosettes were obtained from pale-green *clpp3-1* plants (initially grown in heterotrophic conditions and then transferred to soil) and soil-grown wild-type plants

Table I. *Stoichiometry of Clp subunits determined by MS analysis and the QconCAT technique*

Molar amounts are derived from peak area ratios between the endogenous Clp peptides and 100 fmol of spiked stable isotope-labeled Clp-QconCAT peptides with three technical replicates. ClpP4 could not be quantified in the wild type or in *clpp3-1* samples. Stoichiometry was calculated by normalization against the molar amounts of ClpR4. nd, Not determined.

Subunit	Core[a]		Rings[b]		Core + Rings		Core[c]
	Wild Type	*clpp3-1*	Wild Type	*clpp3-1*	Wild Type	*clpp3-1*	Olinares et al. (2011a)
ClpP3	1.0	0	0.6	0	0.8	0.0	1.0
ClpP4	nd	nd	nd	nd	nd	nd	2.4
ClpP5	3.4	3.9	3.4	8.0	3.4	7.3	2.8
ClpP6	0.9	1.4	0.9	1.5	0.9	1.5	1.1
Sum for P-ring	5.3	5.3	4.9	9.5	5.1	8.8	7.3
ClpP1	2.9	4.9	3.1	5.5	3.0	5.4	3.1
ClpR1	1.0	0.6	1.2	1.0	1.1	0.9	1.2
ClpR2	0.8	0.4	1.0	0.9	0.9	0.8	1.1
ClpR3	0.8	1.8	1.2	1.9	1.0	1.9	1.0
ClpR4	1.0	1.0	1.0	1.0	1.0	1.0	1.0
Sum for R-ring	6.5	8.8	7.5	10.2	7.0	10.0	7.4

[a]From the 450- to 250-kD mass range. [b]From the 250- to 150-kD mass range. [c]Affinity-purified ClpPR complexes using StrepII-ClpR4- and StrepII-P3-complemented Arabidopsis null mutant lines.

(Fig. 9A), both with 20 leaves. Total leaf proteomes were extracted with SDS, and each proteome was separated by SDS-PAGE and visualized by Coomassie staining (Fig. 9B). Each gel lane was excised in 20 slices, followed by in-gel trypsin digestion and protein identification by nano-LC-tandem mass spectrometry (MS/MS). Three biological replicates per genotype were analyzed, resulting in 120 MS/MS runs and 799,375 acquired MS/MS spectra; proteins were identified, and quantified MS data were searched and filtered (Supplemental Fig. S2; Supplemental Table S3). This resulted in the identification of 2,313 proteins, quantified as 1,993 individual proteins and 123 protein groups. These groups contained closely related proteins that were identified with peptides, most of which also matched to homologs (Friso et al., 2011). Based on our recent reference Arabidopsis chloroplast proteome (Huang et al., 2013), 918 proteins were chloroplast localized, representing 63% of the protein mass in *clpp3-1* and 69% in the wild type. This reduced chloroplast mass was due to a 50% reduction in lumenal mass and 26% in thylakoid protein mass (Supplemental Table S4). The average pairwise correlation coefficients among the three biological replicates within the wild-type and *clpp3-1* data sets were 0.990 and 0.983, respectively, indicating high reproducibility between the independent replicates for each genotype. Principal component analysis also showed that the variation between genotypes was larger than between replicates within each genotype (Fig. 9C). Together, these findings show that the quantitative proteome data are of high quality, with little noise, and that *clpp3-1* has a measurable proteome phenotype.

Significance Analysis for Determining Differentially Expressed Proteins

To determine which proteins/protein groups were differentially expressed in *clpp3-1* relative to the wild type, two statistical tools, QSpec (Choi et al., 2008) and GLEE (A. Poliakov, L. Ponnala, P.D. Olinares, and K.J. van Wijk, unpublished data), were employed. These tools were specifically developed for significance analysis of large-scale spectral counting experiments, and both have their merits (for discussion, see Supplemental Text S1). Figure 9D compares the results of the significance analyses of the total leaf data sets using QSpec (Bayes factor $>$ 10) and GLEE ($P < 0.01$). A total of 148 of the plastid-localized proteins and 64 extraplastidic proteins passed both statistical tests (Supplemental Table S3). These extraplastidic proteins were located in diverse subcellular compartments and did not show any functional trends; this indicates the lack of a specific extraplastidic phenotype in *clpp3-1*. In the remainder of this paper, therefore, we will focus on the effects on the plastid proteome and the differentially accumulating plastid proteins (Table II). Immunoblot analysis for a number of thylakoid and stromal proteins was consistent with the results of the MS-based quantification, providing further support for the reliability of MS-based quantification and statistics (Fig. 10). To evaluate general effects of the loss of ClpP3 on the plastid, we compared the chloroplast protein mass investments (based on the normalized adjusted spectral counts [NadjSPC] of designated chloroplast proteins) across 35 functions between *clpp3-1* and the wild type (Fig. 11).

In the next sections, we discuss the results of the proteome analysis in an effort to (1) determine the molecular chloroplast phenotype of *clpp3-1*, (2) identify potential substrates among the up-regulated proteins, and (3) compare the results with previous quantitative proteome analyses *clpr2-1* (Zybailov et al., 2009a) and *clpr4-1* (Kim et al., 2009) to look for consistency and differences between ClpPR core mutants. We note that, due to the improved experimental workflow and MS acquisition settings, we quantified substantially more proteins in *clpp3-1* than in *clpr2-1* and *clpr4-1* (for more information

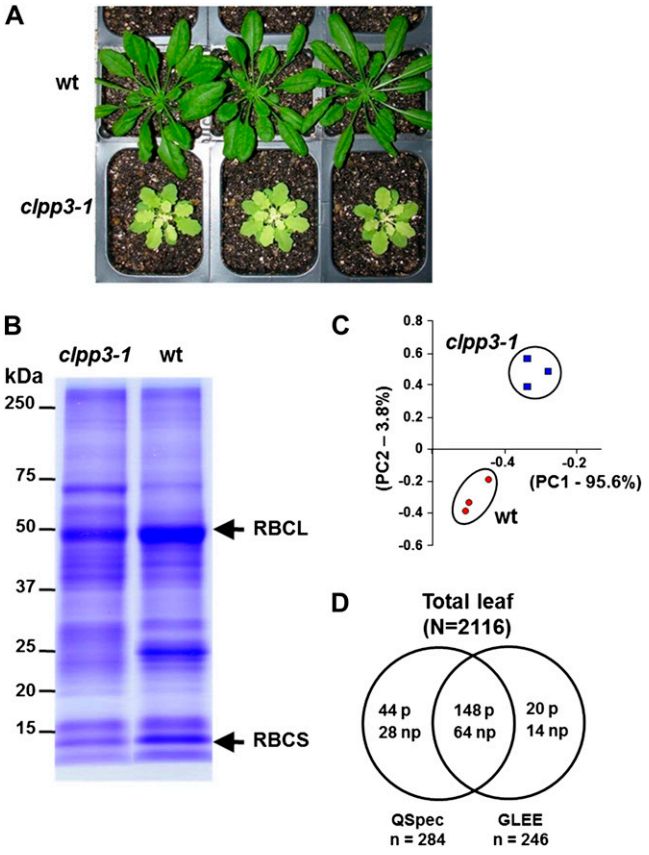

Figure 9. Large-scale spectral count-based comparative proteomics of the *clpp3-1* mutant. A, The *clpp3-1* and wild-type (wt) plants used for proteome analysis. Wild-type (Columbia-0) plants were grown on soil for 40 d under a short-day cycle (10-h/14-h light/dark) at 100 μmol photons m^{-2} s^{-1}. Homozygous *clpp3-1* plants were initially grown on agar plates with one-half-strength Murashige and Skoog medium and 2% Suc under short-day conditions at 40 μmol photons m^{-2} s^{-1} and then transferred to soil after 70 d and grown under a short-day cycle at 100 μmol photons m^{-2} s^{-1} for another 40 d. B, One-dimensional SDS-PAGE gel separation (biological replicate 1) of the total leaf proteomes from *clpp3-1* and the wild type. Rubisco large subunit (RBCL) and Rubisco small subunit (RBCS) are indicated. C, Principal component (PC) analysis of the quantified proteomes of the wild type (circles) and *clpp3-1* (squares). The symbols in the principal component analysis plot represent each of the biological replicates for each of the genotypes. PC1 and PC2 explained 95.6% and 3.8%, respectively, of the total variation. D, Comparison of leaf proteins determined to be significantly expressed in *clpp3-1* relative to the wild type. This includes proteins that have Bayes factor > 10 for QSpec or $P < 0.01$ for GLEE. np, Not plastid; p, plastid-localized proteins. [See online article for color version of this figure.]

on how this improvement was accomplished, see Supplemental Text S1; Supplemental Fig. S3; Supplemental Table S5).

Reduced Photosynthetic Capacity in *clpp3-1*

About 100 proteins involved in the dark and light reactions of photosynthesis were quantified. The overall protein mass of the thylakoid-bound photosynthetic apparatus was decreased by 30% (Fig. 11A). Nearly 40 proteins in the thylakoid photosynthetic apparatus were significantly down-regulated (Table II). These included proteins of each of the five thylakoid complexes (PSI and PSII, cytochrome b_6f, ATP synthase, and NADH dehydrogenase [NDH]). An interesting exception was LHCI-5, which was nearly 5-fold up-regulated. LHCI-5 is a low-abundance protein shown to loosely associate with PSI (Ganeteg et al., 2004) and interacts with the light-harvesting complex I at the Lhca2/Lhca3 site (Lucinski et al., 2006). The NDH-PSI supercomplex was absent in knockout lines of LHCI-5, indicating a potential role for LHCI-5 in mediating the NDH and PSI association (Peng et al., 2010). Related, stromal CRR6 (for chlororespiratory reduction6), involved in assembly of the NDH complex (Munshi et al., 2006), was approximately 4-fold up-regulated (Table II). The overall mass of the Rubisco complex was decreased by 40% (Fig. 11A), consistent with the visible loss of Rubisco subunits on the Coomassie-stained gel (Fig. 9B). Indeed, down-regulation of the small and large subunits of Rubisco was statistically significant (Table II). Surprisingly, the mass of the rest of the Calvin cycle enzymes was not affected in *clpp3-1* (Fig. 11A), and none of the individual proteins was significantly affected, with the exception for one of the isoforms of fructose bisphosphate aldolase (SFBA1; At2g21330), which was 50% up-regulated. SFBA1 was found associated in significant amounts with plastoglobules (PGs; Kessler and Schnell, 2006; Ytterberg et al., 2006), which may explain its up-regulation.

Up-Regulation of the PG Proteome Indicates a Stressed Chloroplast in *clpp3-1*

PGs are thylakoid-associated lipoprotein particles that serve as compartments for the synthesis, storage, and degradation of prenyl lipids and thylakoid membrane remodeling (Bréhélin et al., 2007; Lundquist et al., 2012). The total mass of PG proteins increased 2.6-fold (Supplemental Table S4). As structural proteins, fibrillins maintain the PG coat and likely control PG size, but they may have metabolic functions (Singh and McNellis, 2011). Out of the seven PG-localized fibrillins, three (FBN1a, FBN1b, and FBN8) were significantly 3- to 15-fold up-regulated in *clpp3-1*. PG-localized metabolic enzymes NADH dehydrogenase, carotenoid dioxygenase, and ABC1 kinase3 were also strongly up-regulated (Table II). This is in striking agreement with coexpression analysis based on mRNA abundance, which showed that these three PG enzymes were part of the same coexpression module as the ClpPR core proteins (Lundquist et al., 2012).

Effects on Plastid Gene Expression and Protein Homeostasis

Figure 11B summarizes the effects on plastid gene expression and protein homeostasis. Proteins (in total,

Table II. *Chloroplast-localized proteins that are significantly up-regulated or down-regulated in* clpp3-1 *plants relative to the wild type*

Chloroplast-localized proteins that passed the significance analyses for both QSpec (Bayes factor > 10) and GLEE ($P < 0.01$) at the 5% false discovery rate threshold are shown. Subplastidial location: E, envelope; IE, inner envelope membrane; IES, inner envelope membrane associated, stroma side; L, lumen; S, stroma; TI, thylakoid membrane, integral bound; TL, thylakoid membrane associated, lumenal side; TS, thylakoid membrane associated, stroma side.

Accession	Protein Annotation	Location	Function	*clpp3*/Wild Type[a]	Direction[b]		
					clpp3-1	*clpr2-1*	*clpr4-1*
ATCG00340.1	psaB, subunit Ib	TI	PSI	0.7	D		
AT4G02770.4	psaD-1,2 (subunit II)	TS	PSI	0.6	D		D
AT1G03130.1							
AT5G64040.1	psaN, TAT LTP	TL	PSI	0.6	D		D
AT4G28750.1	psaE-1, subunit IV	TS	PSI	0.5	D		
AT1G55670.1	psaG, subunit V	TI	PSI	0.4	D		
AT1G31330.1	psaF, subunit III	TI	PSI	0.5	D	D	D
AT4G12800.1	psaL, subunit XI	TI	PSI	0.5	D		D
AT1G52230.1	psaH-2, subunit VI	TI	PSI	0.4	D		D
AT1G08380.1	psaO, subunit O	TI	PSI	0.4*	D		
AT1G61520.1	LHCI-3 CAB4	TI	PSI antennae	0.7	D	D	
AT1G45474.1	LHCI-5	TI	PSI-NDH interaction	4.7	U		
ATCG00020.1	psbA D1 protein	TI	PSII	0.6	D		
ATCG00270.1	psbD D2 protein	TI	PSII	0.6	D	D	
ATCG00280.1	psbC CP43	TI	PSII	0.7	D	D	D
ATCG00680.1	psbB CP47	TI	PSII	0.5	D	D	D
ATCG00580.1	psbE cytb559a	TI	PSII	0.4	D		
AT4G21280.1	OEC16 (PsbQ)	TL	PSII	0.5	D		D
AT4G05180.1	OEC16-like (PsbQ-like)	TL	PSII	0.1	D	D	D
AT1G06680.1	OEC23 (PsbP)	TL	PSII	0.5	D	D	
AT3G55330.1	OEC23-like (PsbP-like)	TL	PSII	0.3*	D		
AT5G66570.1	OEC33 (PsbO)	TL	PSII	0.5	D	D	D
AT3G50820.1	OEC33-like (PsbO)	TL	PSII	0.5	D	D	D
AT2G34420.1	LHCII-1.5	TI	PSII	0.4	D		
AT3G27690.1	LHCII-2.3, LHCII-2.2, LHCII-2.1	TI	PSII antennae	0.7	D	D	
AT2G05070.1							
AT2G05100.1							
AT3G08940.2	LHCII-4.2, CP29	TI	PSII antennae	0.6	D		
AT4G10340.1	LHCII-5, CP26	TI	PSII antennae	0.7	D	D	
AT1G15820.1	LHCII-6, CP24	TI	PSII antennae	0.7	D		
AT3G47070.1	Thylakoid phosphoprotein (TSP9)	TS	Photosystem state transition	0.3*	D		
ATCG00540.1	petA, cytochrome *f*	TI	Cytochrome b_6/f	0.5	D		D
ATCG00720.1	petB, cytochrome b_6	TI	Cytochrome b_6/f	0.4	D		D
AT4G03280.1	petC, Rieske Fe-S protein	TL	Cytochrome b_6/f	0.6	D		D
ATCG00120.1	CF1a, atpA	TS	ATP synthase	0.8	D	D	D
AT4G04640.1	CF1y, atpC	TS	ATP synthase	0.6	D		
ATCG00470.1	CF1e, atpE	TS	ATP synthase	0.7	D		D
ATCG01100.1	NDH A (NDH-1)	TI	NDH complex	0.1	D		
AT2G39470.1	NDH subunit PPL2	TL	NDH complex	0.4	D		
ATCG01110.1	NDH H (NDH-7)	T	NDH complex	0.3	D		
AT2G47910.1	CRR6	S	NDH complex assembly	3.7*	U		
ATCG00490.1	Rubisco large subunit (RBCL)	S	Calvin cycle	0.5	D	D	D
AT5G38430.1	Rubisco small subunit 1b (RBCS-1b)	S	Calvin cycle	0.5	D	D	D
AT5G38410.1	Rubisco small subunits 3b and 2b	S	Calvin cycle	0.4	D	D	D
AT5G38420.1	(RBCS-3B, RBCS-2B)						
AT1G67090.1	Rubisco small subunit 4 (RBCS-4)	S	Calvin cycle	0.6	D		D
AT2G21330.1	Fructose bisphosphate aldolase1 (SFBA-1)	S	Calvin cycle and PG?	1.4	U	U	
AT4G22240.1	Fibrillin1b (FBN1b)	PG	PG structure/metabolism	15.5	U	U	U
AT4G04020.1	Fibrillin1a (FBN1a)	PG	PG structure/metabolism	4.3	U	U	
AT2G46910.1	Fibrillin8 (FBN8)	PG	PG structure/metabolism	3.3*	U		
AT1G79600.1	ABC1 kinase3 (ABC1K3)	PG	PG metabolism	10.6*	U		U
AT4G19170.1	Carotenoid cleavage dioxygenase (CCD4)	PG	PG metabolism	4.1*	U		
AT5G08740.1	NADH dehydrogenase (NDC1)	PG	PG metabolism	3.4*	U		
AT5G42650.1	Allene oxide synthase (AOS)	PG	PG metabolism	2.2	U		D

(*Table continues on following page.*)

Table II. (*Continued from previous page.*)

Accession	Protein Annotation	Location	Function	*clpp3*/Wild Type[a]	Direction[b]		
					clpp3-1	*clpr2-1*	*clpr4-1*
AT1G06950.1	Tic110	IE	Protein targeting	2.1	U	U	
AT4G01800.1	cpSecA	TS	Protein targeting	2.4	U		
AT4G14870.1	cpSecE	TI	Protein targeting	4.4*	U		
AT5G15450.1	ClpB3	S	Protein (un)folding	5.5	U	U	U
AT4G24280.1 AT5G49910.1	cpHSP70-1, cpHSP70-2	S	Protein folding	2.5	U	U	U
AT2G04030.1	cpHSP90	S	Protein folding	2.4	U	U	U
AT2G28000.1	Cpn60-α-1	S	Protein folding	2.1	U	U	
AT3G13470.1 AT1G55490.1	Cpn60-β-1,2	S	Protein folding	2.2	U	U	
AT5G56500.2	Cpn60-β-3	S	Protein folding	8.3*	U	U	
AT2G44650.1	Cpn10-1	S	Protein folding	2.7	U		
AT5G20720.1	Cpn21 (also Cpn20)	S	Protein folding	1.5	U		
AT5G55220.1	Trigger factor	S	Protein folding	1.7	U		
AT3G62030.1	Peptidylprolyl isomerase ROC4	S	Protein folding	1.5	U	U	
AT5G13410.1	FKBP-type isomerase	TL	Protein folding	0.3	D		
AT5G42390.1	Stromal processing peptidase (SPP)	S	Protease	5.5	U		
AT5G05740.1	EGY2 metalloprotease	T	Protease	3.4*	U		
AT1G73990.1	SppA	TI	Protease	6.1	U		
AT3G19170.1	PreP1, zinc metalloprotease	S	Protease	2.4	U	U	U
AT4G30920.1	Leucyl aminopeptidase (LAP2)	S	Protease	3.1	U		
AT5G35970.1	DEAD box DNA helicase related	S	DNA binding	4.0*	U		
AT3G07430.1	YMLG1	S	DNA-nucleoid distribution	3.5*	U		
AT1G80480.1	PRLI-interacting factor L (pTAC17)	S	DNA binding	3.2*	U		
AT2G02740.1	Why3 (pTAC11)	N	Transcription regulation	6.7	U		
AT5G14260.1	SET domain-containing protein	S	Transcription regulation	2.0	U		
AT4G09040.1	RNA recognition motif (RRM) protein	S	RNA	4.6*	U		
AT4G16390.1	PPR protein P67 (SVR7)	S	RNA	3.8	U		
AT1G70070.1	DEAD/DEAH box helicase	S	RNA	4.0*	U		
AT1G59990.1	DEAD box RNA helicase (RH22)	U	RNA	4.0*	U		
AT5G63420.1	RNase J homolog	S	RNA processing	3.6*	U		
AT5G26742.1	DEAD box RNA helicase (RH3)	N	RNA	2.4	U	U	U
AT5G46580.1	Pentatricopeptide repeat (PPR)	U	RNA	8.9*	U		
AT3G18680.1	Uridylate kinase; Defect psaA/B mRNA (DPT1)	S	RNA	3.7*	U		
AT3G13740.1	RNase III protein	U	RNA	3.6*	U		
ATCG00830.1 ATCG01310.1	50S ribosomal protein L2A and L2B	S	Protein synthesis	0.4	D		
AT3G44890.1	50S ribosomal protein L9	S	Protein synthesis	0.6	D		
AT5G40950.1	50S ribosomal protein L27	S	Protein synthesis	0.4	D		
AT3G20230.1	50S ribosomal protein L18	S	Protein synthesis	4.3*	U		
AT4G29060.1	pETs (fusion of EF-Ts and PSRP-7)	S	Protein synthesis	1.4	U	U	U
AT5G13650.1	Elongation factor protein, type A/bipA like (SVR3)	S	Protein synthesis	3.5	U	U	U
AT4G20360.1	Elongation factor Tu (EF-Tu-1)	S	Protein synthesis	1.7	U	U	U
AT1G62750.1	Elongation factor Tu-G (EF-G; sco1)	S	Protein synthesis	2.3	U	U	
AT4G33760.1	tRNA synthetase class II (D, K, and N)	S	Protein synthesis	4.9	U		
AT5G49030.1	Ile-tRNA synthetase class II (OVA2)	S	Protein synthesis	5.0	U		
AT3G48110.1	Gly-tRNA synthetase (GlyRS-2; EDD1)	S	Protein synthesis	2.2	U		
AT1G16720.1	HCF173, translation D1 protein	S	Protein synthesis	2.3	U		
AT2G36250.1	FtsZ2.1	S	Plastid division	2.4	U		U
AT4G16155.1	E3, dihydrolipoamide dehydrogenase2 (ptlpd2)	S	Fatty acid synthesis	2.9*	U		
AT2G38040.1	Carboxyltransferase (CT) α-subunit ACCase	IES	Fatty acid synthesis	0.5	D		
AT5G35360.1	Biotin carboxylase (BC), part of the ACCase complex	IES	Fatty acid synthesis	2.2	U		
AT4G14070.1	Plastidial long-chain acyl-CoA synthetase	E	Fatty acid synthesis	3.0	U		
AT2G30200.1	Malonyl-CoA:acyl carrier protein transacylase	S	Fatty acid synthesis	3.0	U		

(*Table continues on following page.*)

Table II. (*Continued from previous page.*)

Accession	Protein Annotation	Location	Function	*clpp3*/Wild Type[a]	Direction[b]		
					clpp3-1	*clpr2-1*	*clpr4-1*
AT3G22960.1	Pyruvate kinase1	S	Fatty acid synthesis	1.8	U		
AT5G60600.1	4-Hydroxy-3-methylbutyl diphosphate synthase (HD)	TS	MEP pathway	3.2	U	U	U
AT4G27440.1	PORB, constitutive expression	TS	Tetrapyrrole synthesis	0.4	D		
AT4G31990.1	Asp aminotransferase (AAT1/Asp5)	S	Amino acid metabolism	2.8	U		U
AT5G10920.1	Argininosuccinate lyase (AtArgH)	U	Amino acid metabolism	2.8*	U		
AT4G33510.1	3-Deoxy-D-arabino-heptulosonate 7-P synthase2 (DHS2)	U	Amino acid metabolism	3.1	U		
AT4G29840.1	Thr synthase (MTO2)	S	Amino acid metabolism	2.5	U		
AT1G18500.1 AT1G74040.1	2-Isopropylmalate synthase (IMS)	S	Amino acid metabolism	2.6	U		
AT4G13430.1	Isopropylmalate isomerase large subunit	S	Amino acid metabolism	2.9	U		
AT3G58610.1	Ketol acid reductoisomerase	S	Amino acid metabolism	1.6	U		U
AT2G43750.1	Cys synthase	S	Amino acid metabolism	0.5	D		
AT5G48960.1	5′-nucleotidase	S	Nucleotide metabolism	3.0*	U		
AT5G53460.1	NADH-GOGAT or NADH-Glu synthase (GLT)	S	Nitrogen metabolism	21.9	U		U
AT5G04140.1	Ferredoxin-GOGAT1	S	Nitrogen metabolism	1.4	U	U	U
AT1G32900.1	Starch synthase	S	Starch synthesis	3.7	U		
AT5G24300.1	Starch synthase1 (SS1)	S	Starch synthesis	2.3	U		
AT5G19220.1	ADP-Glc pyrophosphorylase (ADG2)	S	Starch synthesis	2.2	U		
AT1G69830.1	α-Amylase (AMY3)	S	Starch degradation	3.2	U	U	
AT5G26570.1	Phosphoglucan water dikinase (PWD)	S	Starch degradation	2.4	U		
AT1G10760.1	Water dikinase (Sex1)	S	Starch degradation	1.5	U	U	
AT1G04420.1	Aldo/keto reductase family protein	S	Sugar metabolism	2.4	U		
AT1G29900.1	Carbamoylphosphate synthetase	S	Pyrimidine synthesis	2.1	U		U
AT3G06730.1	Thioredoxin Z	S	Reactive oxygen species defense	3.1*	U		
AT4G23100.1	γ-Glutamyl-Cys synthetase (GSH1)	S	Reactive oxygen species defense	3.8	U		
AT3G54660.1	Gluthatione reductase	S	Reactive oxygen species defense	4.0	U		
AT3G26060.1	Peroxiredoxin Q (Prx Ql likely lumenal)	TL	Reactive oxygen species defense	0.3	D		
AT5G01600.1	Ferritin-1	S	Iron storage	4.4*	U		U
AT1G80300.1	ATP/ADP translocator1 (NTT1)	IE	Metabolite transporter	5.9*	U		
AT1G15500.1	ATP/ADP translocator2 (NTT2)	IE	Metabolite transporter	9.6*	U		U
AT5G24650.1	Inner membrane translocase subunit (Tim17/22)	E	Metabolite transporter	3.3*	U		
AT3G49560.1	Inner membrane translocase subunit (Tim17)	E	Metabolite transporter	3.3*	U		
AT5G13420.1	Transaldolase1	S	OPP	3.0*	U		
AT1G64190.1	6-Phosphogluconate dehydrogenase1	S	OPP	2.9*	U		
AT4G32520.1	Ser hydroxymethyltransferase (SHM3)	S	C1 metabolism	3.2*	U		
AT5G20250.1	Raffinose synthase or seed inhibition protein Sip1	U	Unknown	7.5*	U		
AT2G39670.1	Radical SAM-containing protein	S	Unknown	4.0*	U		
AT1G71500.1	Rieske [2Fe-2S] domain	T	Unknown	0.4	D		
AT2G42220.1	Rhodanese-like protein	T	Unknown	0.3	D		
AT5G51110.1	Unknown protein	S	Unknown	7.4*	U		
AT2G44640.1	Unknown protein	E	Unknown	3.9*	U		
AT3G04550.1	Unknown protein	S	Unknown	3.3*	U		
AT3G01060.1	Unknown protein (likely plastid nucleoid)	U	Unknown	2.7*	U		
AT1G44920.1	Unknown protein	U	Unknown	2.5	U		
AT3G61870.1	Unknown protein (integral membrane)	E	Unknown	3.2	U		

(*Table continues on following page.*)

Table II. (*Continued from previous page.*)

Accession	Protein Annotation	Location	Function	*clpp3*/Wild Type[a]	Direction[b]		
					clpp3-1	*clpr2-1*	*clpr4-1*
AT2G26340.1	Unknown protein	T	Unknown	0.4*	D		
AT5G08050.1	Unknown protein (DUF1118)	T	Unknown	0.4*	D		
AT1G74730.1	Unknown protein (DUF1118)	T	Unknown	0.3*	D		

[a]Protein accumulation ratio between *clpp3-1* and the wild type (three biological replicates each) obtained from NadjSPC (leaf). Ratios marked with asterisks had zero spectral count in one or more replicates, with fold change estimated by imputation for zero values from QSpec analysis. [b]Based on the *clpp3-1*/wild-type accumulation ratios, the protein can be up-regulated (U) or down-regulated (D). These were derived from this study (*clpp3- 1* dataset), Zybailov et al. (2010; *clpr2-1* dataset), and Kim et al. (2010; *clpr4-1* dataset).

268) involved in these processes were grouped in 11 functional classes. This showed that overall protein mass investments in plastid ribosomes, the Clp system, protein assembly, and DNA-related functions were unchanged in *clpp3-1*. In contrast, overall protein mass investments in protein (un)folding, tRNA synthases, protein synthesis, and other proteolytic systems were 2-fold increased. Furthermore, protein-targeting machinery and proteins involved in RNA metabolism also overaccumulated in *clpp3-1* (Fig. 11B).

This general pattern was also reflected in the significantly affected proteins across these functions (Table II). More than 40 proteins were significantly affected, all of which were up-regulated, except for a lumenal isomerase (consistent with the reduction of the lumenal proteome) and three 50S ribosomal proteins, which were down-regulated. The up-regulated proteins include the chloroplast chaperones CPN60α,β (Fig. 10), CPN10,20, cpHSP70-1,2, and cpHSP90, which play crucial roles in protein folding and maturation (Boston et al., 1996; Wandinger et al., 2008). ClpB3, the chloroplast homolog of the bacterial ClpB protein (Myouga et al., 2006), was 5-fold up-regulated. ClpB3 is involved in unfolding aggregated proteins together in the cpHSP70 system (Goloubinoff et al., 1999; Haslberger et al., 2008). The up-regulation of these chaperone systems was also observed in other Clp mutants (Rudella et al., 2006; Kim et al., 2009; Zybailov et al., 2009a). ROC4, an abundant stromal peptidylprolyl isomerase (Peltier et al., 2006; Zybailov et al., 2008) with in vitro rotamase activity (Lippuner et al., 1994), also overaccumulated. In summary, loss of ClpP3 accumulation clearly resulted in major protein-folding stress, perhaps due to the accumulation of unwanted proteins.

Out of the 25 other detected proteases, just three stromal proteases/peptidases and two thylakoid proteases were significantly affected in *clpp3-1*. Stromal Zn^{2+}-protease PreP1, stromal processing peptidase (SPP), and leucyl aminopeptidase2 (LAP2) were 2.4- to 5.5-fold up-regulated (Table II). PreP1 was suggested to be involved in the degradation of cleaved chloroplast transit peptides (Bhushan et al., 2005; Ståhl et al., 2005; Glaser et al., 2006), whereas stromal SPP is involved in the transit peptide removal of most nucleus-encoded, chloroplast-targeted proteins (Richter and Lamppa, 1998, 1999). LAP2 belongs to the family of soluble aminopeptidases (Walling, 2006), and it was recently suggested that LAP2 also moonlights as a chaperone in the chloroplast (Scranton et al., 2012). The two affected thylakoid proteases are EGY2 and SPPA, which are 3- and 6-fold increased, respectively, in *clpp3-1*. EGY2 is an ATP-independent intramembrane protease in the Site-2 protease family (Chen et al., 2012) and is a paralog of the

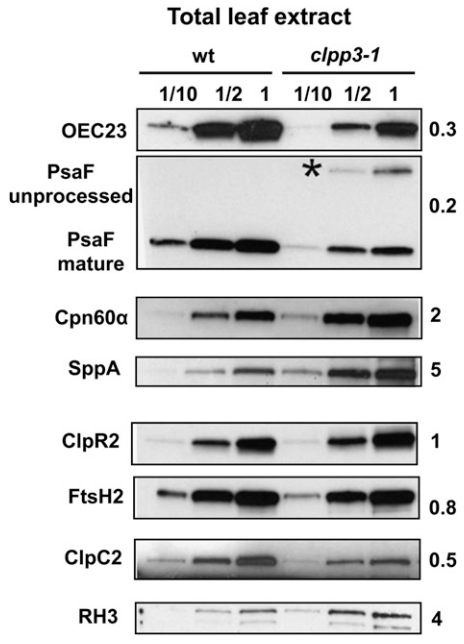

Figure 10. Confirmation of quantitative proteome analysis of total leaf extracts of the wild type (wt) and *clpp3-1* by immunoblotting. Immunoblot analysis is shown for titrations (indicated as 1/10, 1/2, and 1) of total leaf protein extracts from the wild type and *clpp3-1* used in the proteome analysis. Membranes were probed with antibodies generated against different proteins of PSI and PSII (OEC23, oxygen-evolving complex component of PSII; PsaF, a small peripheral subunit of PSI); chaperones and proteases (ClpC2, stromal chaperone; ClpR2, subunit of the Clp protease complex; FtsH2, thylakoid protease of the zinc metalloprotease family; Cpn60α; SppA, ATP-independent, light-induced Ser-type thylakoid protease), and the stromal RNA helicase RH3. 1× = 20 μg. The asterisk indicates a precursor form of PsaF that is also observed in *clpr2-1* (Rudella et al., 2006). The *clpp3-1*/wild-type ratio is indicated on the right side.

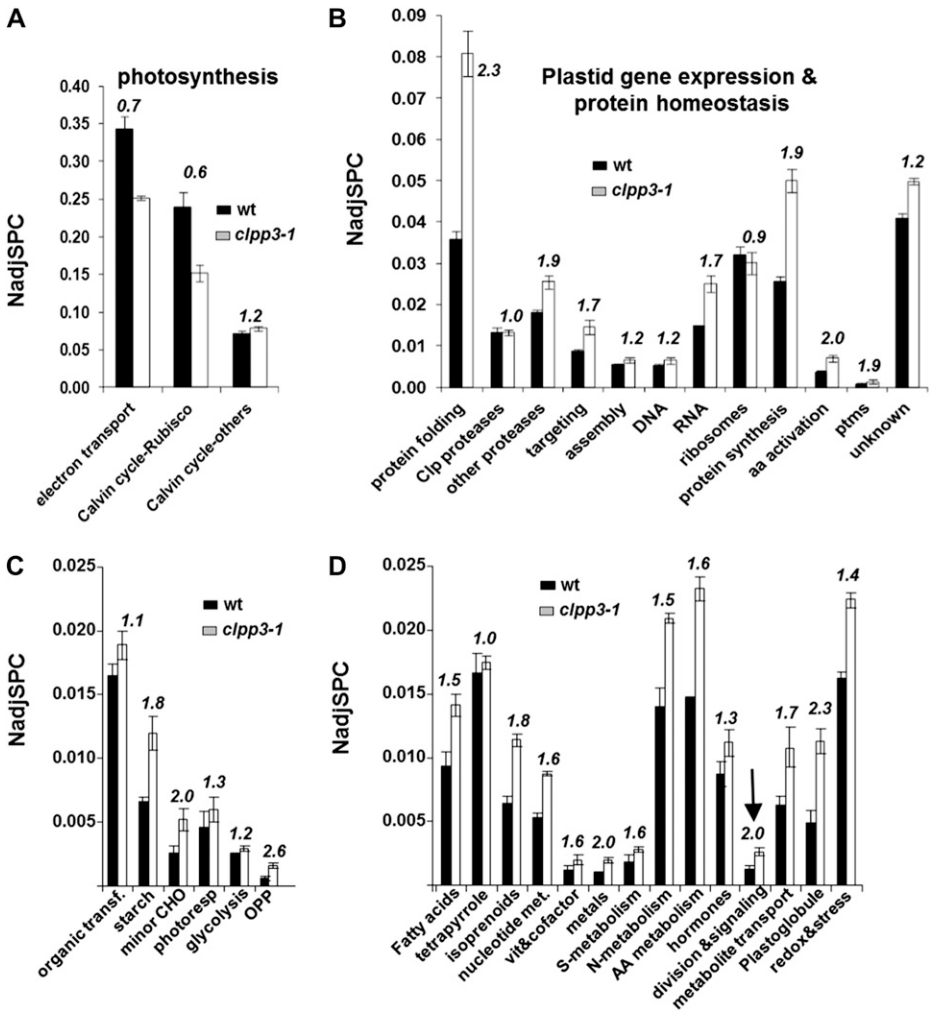

Figure 11. Protein mass investment based on NadjSPC in specific plastid functions in the wild type (wt) and *clpp3-1*. Error bars correspond to the SD across three biological replicates. The *clpp3-1*/wild-type ratios are also indicated for each function. Black bars indicate the wild type, and gray bars represent *clpp3-1*. A, Investment in photosynthesis in the thylakoid and stroma (Calvin cycle). B, Investments in plastid gene expression and protein homeostasis. Proteins (in total, 268) involved in these processes were grouped in 11 functional classes and proteins of unknown function: plastid ribosomes (53 proteins), the Clp system (12 detected proteins), protein assembly (20 proteins) and DNA-related functions (10 proteins), protein (un)folding (23 proteins), amino acid activation (22 tRNA synthases), protein synthesis (21 proteins), other proteolytic systems (25 proteins), protein-targeting machinery (22 proteins), proteins involved in RNA metabolism (51 proteins), and posttranslational modifiers (ptms; 9 proteins). C, Investments in primary carbon metabolism including the metabolism of starch and minor carbohydrates, photorespiration, glycolysis, the OPP pathway, and organic transformation (dominated by the abundant carbonic anhydrases and malate dehydrogenase). D, Investments in other functions. AA, Amino acid; CHO, carbohydrate; met, metabolism; ptms, posttranslational modification (e.g. kinases); vit, vitamins.

better-characterized EGY1 thylakoid-bound metalloprotease that is crucial for thylakoid development and the accumulation of chlorophyll-containing proteins (Chen et al., 2005). SppA is a light stress-induced, thylakoid-bound, ATP-independent Ser-type protease with unknown substrates (Lensch et al., 2001). Interestingly, the very abundant thylakoid FtsH protease complex (FtsH1, FtsH2, FtsH5, and FtsH8; Liu et al., 2010b; Kato et al., 2012), robustly quantified with many MS/MS spectra (114, 499, 528, and 146 for FtsH1, FtsH2, FtsH5, and FtsH8, respectively; Supplemental Table S3), was not significantly affected (between 0.8- and 1.2-fold). Immunoblot analyses confirmed the fold changes of SppA, whereas the abundance levels of ClpR2 and the thylakoid protease FtsH2 were unchanged, consistent with the MS-based quantifications (Fig. 10). Thus, the loss of Clp protease capacity specifically affects a subset of chloroplast proteases, indicative of a controlled protease network.

pTAC11 (WHY3) and pTAC17, initially identified in transcriptionally active chromosome (TAC) fractions (Pfalz et al., 2006), were 7- and 3-fold up-regulated in *clpp3-1*, respectively. In particular, pTAC11, but not pTAC17, is strongly enriched in nucleoids (Majeran et al., 2012; Huang et al., 2013). The function of pTAC17 is unknown, but sequence analysis suggests that it may be involved in DNA repair; importantly, we recently identified it as a candidate substrate for the substrate selector ClpS (K. Nishimura, Y. Asakura, G. Friso, J. Kim, S.H. Oh, H. Rutschow, L. Ponnala, and K.J. van Wijk, unpublished data). Plastid pTAC11 is a member of the Whirly family of multifunctional RNA- and DNA-binding proteins located in mitochondria and plastids (Krause et al., 2005). Members of the Whirly family are involved in organelle genome stability and quality control and, perhaps, RNA metabolism (Prikryl et al., 2008; Maréchal et al., 2009; Cappadocia et al., 2012). A SET domain-containing protein (At5g14260) was also significantly overaccumulating in *clpp3-1*; the SET domain is frequently found in DNA-interacting proteins. Finally, a DEAD box DNA helicase likely involved in DNA folding and YMLG1 were up-regulated. YMLG1 (Kabeya et al., 2010) is involved in the distribution of nucleoids in chloroplast. Together, these results suggest that the loss of Clp protease function has an impact on the plastid chromosome.

Nine proteins (likely) involved in RNA metabolism were significantly up-regulated in *clpp3-1* (Table II).

These include PPR and RRM proteins, RNase RNase J and an uncharacterized RNase, as well as three DEAD/DEAH RNA helicases, including RH22, RH3, and uridylate kinase (DPT1). Bacterial RNase J has been implicated in 16S ribosomal RNA maturation and ribosome assembly (Britton et al., 2007), and the Arabidopsis RNase J is essential for embryogenesis (Meinke et al., 2009). Recently, we characterized RNA helicase3 (RH3) as a plastid RNA splice factor, also affecting ribosome biogenesis (Asakura et al., 2012). PPR protein SVR7 was identified as a suppressor of the FTSH2 protease VAR2 and has a chloroplast ribosomal RNA phenotype (Liu et al., 2011a). Uridylate kinase is involved in post-transcriptional steps of psaA/psaB transcript accumulation (Hein et al., 2009). Thus, loss of Clp protease function also impacts RNA metabolism.

Protein elongation factors EF-Tu, EF-G, TypA/bipA (SVR3), three tRNA synthetases, and the Arabidopsis ortholog of bacterial trigger factor were several fold up-regulated (Table II). *E. coli* trigger factor binds to the 70S exit tunnel and prevents misfolding and aggregation of emerging nascent proteins (Ferbitz et al., 2004). This indicates that loss of Clp protease function leads to a bottleneck in plastid translation.

No Systematic Defect in the Accumulation of Plastid-Encoded Proteins

To determine if *clpp3-1* suffered from a systematic problem in the accumulation of chloroplast-encoded proteins, we evaluated the accumulation of chloroplast-encoded proteins. In total, 53 chloroplast-encoded proteins were identified and constituted 34% of the total chloroplast proteome mass in the wild type but only 23% in *clpp3-1*. Only chloroplast-encoded proteins that are part of the photosynthetic apparatus (25 proteins) were down-regulated, likely reflecting a systematic down-regulation of the photosynthetic apparatus, including nucleus-encoded proteins, rather than a general defect in plastid gene expression. Indeed, accumulation levels of chloroplast-encoded proteins that are not involved in photosynthesis (in total, 28 proteins), including ribosomal proteins, the PEP complex, YCF1 and YCF4, ClpP1, and carboxyltransferase β (part of ACCase), were unchanged (or even up-regulated) in *clpp3-1*. This is an important conceptual result.

Carbon Metabolism

Figure 11C shows the mass investments in primary carbon metabolism, including the metabolism of starch and minor carbohydrates, photorespiration, glycolysis, the oxidative pentose phosphate (OPP) pathway, and organic transformation (dominated by the abundant carbonic anhydrases and malate dehydrogenase). Likely in response to the loss of photosynthetic capacity, the OPP pathway was 2.6-fold up-regulated in *clpp3-1*; indeed, two OPP enzymes significantly increased in *clpp3-1* (Table II). Investment in the metabolism of various minor carbohydrates and well as starch metabolism were also up-regulated (Fig. 11C). Consistently, six enzymes in starch synthesis and degradation were significantly up-regulated, in agreement with observations for the other Clp core mutants, *clpr2-1* and *clpr4-1* (Table II). It is not clear why starch metabolism is up-regulated, but it is perhaps in response to the shortage of reduced carbohydrates produced by the chloroplast.

Strong Up-Regulation of ATP Transporters Suggests That the Chloroplast Is Starved for ATP

Four envelope metabolite transporters were up-regulated in *clpp3-1* (Table II), of which the two nucleoside triphosphate transporters (NTT1 and NTT2) are involved in importing ATP (Reinhold et al., 2007). These NTT isoforms were 6- to 10-fold up-regulated in *clpp3-1*, which is consistent with the strong loss of photosynthetic capacity.

Responses of Other Chloroplast Metabolic Pathways to the Loss of ClpP3

Figure 11D summarizes the investment of other functions in the chloroplast. Investments in metal homeostasis and the function plastid division and signaling were doubled in *clpp3-1*. Specifically, metal homeostasis included three ferritins involved in the storage of iron and two copper chaperones (CCS and CUTA). Up-regulation (4-fold) of ferritin1 was significant (Table II). The increased abundance in plastid division was in particular due to increased levels of the FtsZ family. Investments in several other metabolic pathways (metabolism of fatty acids, isoprenoids, nucleotides, nitrogen, sulfur, and amino acids) were increased by 50%. Consistently, several dozen proteins in these functions were significantly up-regulated, in particular, proteins involved in fatty acid and amino acid metabolism (Table II). In contrast, investment in tetrapyrrole metabolism (chlorophyll, heme, and siroheme) was unchanged in *clpp3-1* (Fig. 11D); indeed, only one protein in tetrapyrrole metabolism was affected in *clpp3-1* (Table II). NADH-GOGAT/GLT1, mostly involved in the assimilation of nitrogen, stands out for its very strong (22-fold) up-regulation. Ferredoxin-GOGAT, primarily involved in the generation of Glu to support the assimilation of photorespiratory ammonium, was also significantly up-regulated in *clpp3-1* (Table II). 4-Hydroxy-3-methylbutyl diphosphate synthase (HDS) controls the methylerythritol phosphate pathway that generates precursors for plastid isoprenoids. HDS was up-regulated in *clpp3-1*, in agreement with the other Clp core mutants, *clpr2-1* (Rudella et al., 2006) and *clpp4-1* (Kim et al., 2009). Interestingly, methylerythritol cyclodiphosphate, the substrate of HDS, elicits the expression of selected stress-responsive nucleus-encoded plastid proteins (Xiao et al., 2012).

Comparison of *clpp3-1* with *clpr2-1* and *clpr4-1* Showed Exceptional Consistency in Proteome Phenotypes

Previously, we carried out comparative proteome analysis of leaf extracts of the *clpr2-1* and *clpr4-1* core mutants. Because the ClpPR subunits assemble in a single functional complex, we postulated that it is likely that the molecular phenotypes should be very similar. Therefore, we determined if the significantly altered proteins in *clpp3-1* were also affected in these core mutants. Indeed, respectively, 36 and 40 proteins were also significantly affected in these mutants, and importantly, for all but one (AOS), these proteins showed similar direction of response (up or down) to *clpp3-1*. This shows that the molecular plastid phenotypes of the three ClpPR core mutants are very similar and also underscores that our workflow was very robust and that our significance analysis did not produce many false positives.

DISCUSSION

Functional and Structural Contributions of ClpPR Subunits to the Chloroplast ClpPR Core Complex

The presence of an extended family of four noncatalytic ClpR proteins and five catalytic ClpP proteins in higher plant chloroplasts suggests specific evolutionary adaptation of the Clp protease system to higher plant plastid/chloroplast metabolism and protein homeostasis. Therefore, in an effort to unravel this adaptation, we and others have aimed to establish the functional and structural contributions of each of the nine different ClpPR subunits to the chloroplast Clp protease in Arabidopsis (for review, see Olinares et al., 2011b). The tetradecameric Clp protease core consists of the heptameric R-ring with ClpP1, ClpR1, ClpR2, ClpR3, and ClpR4 in a 3:1:1:1:1 ratio and one heptameric P-ring with ClpP3, ClpP4, ClpP5, and ClpP6 in a 1:2:3:1 ratio (Olinares et al., 2011a). The stoichiometry and distribution of the ClpPR subunits across and within these two heptameric rings provide an excellent basis for understanding the contribution of each subunit.

Including this study, null mutants for six of the eight nucleus-encoded ClpPR subunits (R1, R2, R4, P3, P4, and P5) have now been obtained and characterized (Koussevitzky et al., 2007; Kim et al., 2009). Moreover, chloroplast-encoded ClpP1 was shown to be essential for shoot development in tobacco (Shikanai et al., 2001; Kuroda and Maliga, 2003). In addition, antisense lines for ClpP4 (Zheng et al., 2006) and for ClpP6 (Sjögren et al., 2006) were investigated that could germinate, develop on soil, and produce seeds; these plants still expressed ClpP4 or ClpP6, albeit at low levels. Downregulation of ClpP4 or ClpP6 resulted in reduced greening, reduced photosynthesis, and delayed development, as expected. In the case of antisense ClpP4, immunoblotting suggested that the subunits in the P-ring decreased more than those of the R-ring, but the assembly state of the subunits was not investigated (Zheng et al., 2006). In the case of antisense ClpP6, using SDS-PAGE gels and immunoblotting did not show consistent changes in ClpPR accumulation levels or in systematic differences between the subunits of the R-ring and the P-ring (except of course for reduced ClpP6; Sjögren et al., 2006). Currently, ClpR3 is the only ClpPR subunit for which no mutant has been described. This subunit is interesting, as it can fully complement the ClpR1 null mutant when ClpR3 is overexpressed (Kim et al., 2009), and ClpR3 protein levels increased in the *clpr1-1* mutant background (Stanne et al., 2009).

Taking this organization and all other experimental data, as well as the primary sequences for the ClpPR proteins, into account, we can describe the following emerging view of the Clp protease core. Both the noncatalytic ClpR and catalytic ClpP subunits make important contributions to Clp core functions with very little structural or functional redundancy. Within the R-ring, ClpR3, but not the other ClpR proteins, can partially substitute for ClpR1. Loss of ClpP1, ClpR2, or ClpR4 results in dramatic chloroplast and leaf developmental phenotypes and is strictly required for flowering, whereas also embryo plastid development is negatively impacted. Within the P-ring, the subunits present in more than one copy (ClpP4 and ClpP5) are absolutely required for embryogenesis, whereas the function of ClpP3 present in one copy is not strictly required for embryogenesis but is strictly required for leaf development and flowering. However, supplementation with sugars (Glc or Suc) can suppress part of the developmental phenotype, unlike in mutants for members of the R-ring (ClpR2 and ClpR4). Whereas antisense lines of ClpP6 show that this subunit is important for chloroplast biogenesis and leaf development, it is not known if null alleles in ClpP6 phenocopy the ClpP3 null allele or the ClpP4 and ClpP5 null alleles. However, given that ClpP6 is present in only one copy, we speculate that a null allele would resemble the ClpP3, ClpR2, or ClpR4 allele.

The Assembly State of the Clp Core without ClpP3

Our results indicate that in *clpp3-1*, a much smaller percentage of ClpPR proteins can effectively assemble into 350- to 400-kD core complexes. Combining the native immunoblot and QconCAT results, the more dominant proteins in the mutant core are ClpR3, ClpP5, ClpP6, ClpP1, and ClpT1, with underrepresentation of ClpP3 (null), ClpP4, ClpR1, ClpR2, and ClpR4. This suggests that a core is assembled with only a subset of ClpPR proteins. Given that ClpP3 is absent and ClpP4 is not well assembled into the Clp core, as compared with ClpP6 in *clpp3-1*, this suggests a significantly modified core complex in *clpp3-1*. Interestingly, when considering both core and individual rings, ClpP5, ClpP6, ClpP1, and ClpR3 each overaccumulated between 2- and 2.5-fold in *clpp3-1* as compared with the wild type. For ClpP6, this could be confirmed by immunoblotting of the native gels, which also showed that ClpP4 levels

increased severalfold. In contrast, accumulation levels of ClpR1, ClpR2, and ClpR4 were unchanged; again for ClpR2, this could be confirmed by immunoblotting of the native gels.

Comparison of the Clp assembly states in *clpp3-1* with the knockdown mutant *clpr2-1* shows that the two mutants have different core complexes. With lower overall levels of ClpR2 in *clpr2-1*, ClpP4 and ClpP6 assemble into the 350-kD complex, but not as efficiently as in the wild type. It appears as if all copies of ClpR2 are used to assemble a wild-type-like core, with the excess of other ClpPR proteins accumulating mostly in heptameric rings. In contrast, in *clpp3-1*, only a subset of the Clp subunits assemble in a core complex with a composition substantially different from the wild type, with the remaining subunits accumulating in heptameric rings.

Double rings for ClpP4 and ClpP6 were observed in *clpp3-1* and *clpr2-1* but not in the wild type. In contrast, ClpR2 assembles in a single ring. This indicates heterogeneity in the P-ring in the mutants. It is unlikely that differential association of ClpT can explain this heterogeneity, because immunoblotting showed ClpT1 only in core complexes and barely in 180- to 200-kD rings. Interestingly, ClpT1 showed an upward shift in SDS-PAGE in the case of *clpp3-1* but not in *clpr2-1*. We do not know what this posttranslational modification represents, but a posttranslational modification search based on MS/MS analysis did not show a particular modification, nor alternative processing or splicing.

Proteomes of ClpR2, ClpR4, and ClpP3 Mutants Show a Consistent Phenotype

A comparative quantitative proteomics analysis of *clpp3-1* (this study) was integrated with our previous comparative proteome analyses of *clpr2-1* (Zybailov et al., 2009a) and *clpr4-1* (Kim et al., 2009) in an effort to (1) determine if there are consistent or unique molecular phenotypes across these different Clp core mutants that may help to explain the function of the Clp protease system and its evolutionary adaptation to the chloroplast, (2) find potential Clp substrates observed as up-regulated proteins that overaccumulated because of their increased lifetime due to reduced Clp protease capacity, and (3) provide a basis for the determination of the chloroplast protease network, through the monitoring of accumulation levels of proteases. Here, we will summarize and discuss our findings in the context of these objectives.

In general, we observed very similar proteome phenotypes between *clppr2-1*, *clpr4-1*, and our analysis here of *clpp3-1*. Due to the much improved workflow for *clpp3-1*, we were able to identify many more significant changes in *clpp3-1* than in the other mutants. The consistent phenotype across these mutants indicates that the activities of each of the ClpPR subunits occur through their contribution to a single ClpPR core complex and not because of the activity of individual subunits per se. Collectively, a clear chloroplast phenotype emerges from these Clp core mutants with nine key characteristics: (1) a strong loss of photosynthetic capacity through a systematic loss of the thylakoid-bound photosynthetic machinery and the Rubisco holocomplex (this is consistent with its pale-green phenotype and delayed growth); (2) strong differential up-regulation of plastoglobular proteins, in particular of module 2 of the plastoglobular coexpression network (Lundquist et al., 2012), indicative of a thylakoid membrane homeostasis problem; (3) up-regulation of a subset of DNA/nucleoid-interacting proteins, most likely involved in DNA/genome quality control; (4) differential effects on RNA metabolism; (5) strong up-regulation of protein translation factors, but not at all of plastid ribosomes; (6) systematic up-regulation of stromal chaperone systems; (7) up-regulation of the chloroplast Sec machinery, suggesting a bottleneck in thylakoid protein insertion; (8) up-regulation of a narrow set of chloroplast proteases; and (9) a limited number of changes in envelope transporters and enzymes involved in primary and secondary metabolism (most can be explained by the loss of ATP/NADPH production). A clear example is the up-regulation of the inner envelope ATP/ADP translocators (NTTs), which import cytosolic ATP into the chloroplast, confirming the reduced ATP-generating capacity in the chloroplast (Reinhold et al., 2007). Finally, the selective decrease in plastid-encoded proteins indicates that there is no systematic defect in plastid gene expression in *clpp3-1*. Only chloroplast-encoded proteins that are part of the photosynthetic apparatus were down-regulated, likely reflecting a systematic down-regulation of the photosynthetic apparatus, including nucleus-encoded proteins. The mechanism for this selective loss of accumulation of chloroplast-encoded protein is unclear but could either be accelerated turnover of thylakoid proteins or a retrograde signaling specifically resulting in down-regulating the expression of thylakoid proteins. Together, this proteome phenotype suggests that the Clp protease system likely has broad substrate specificity and that its general function is essential for chloroplast biogenesis and cannot be replaced by other proteases. Loss of Clp protease capacity specifically affected a subset of chloroplast proteases, indicative of a controlled protease network. Targeted crosses between Clp mutants and other chloroplast protease mutants are in progress in our laboratory to define this network.

The Search for Substrates

An additional motivation for our comparative quantitative proteomics analysis of *clpr2-1*, *clpr4-1*, and *clpp3-1* was to find up-regulated proteins that overaccumulated because of their increased lifetime due to reduced Clp protease capacity. Indeed, we identified 95 statistically significant up-regulated proteins, but in many cases, these can be explained as compensatory responses to the loss of photosynthetic capacity as well as the destabilization of protein homeostasis, resulting in increased levels of chloroplast chaperone systems and selected proteases. However, there are a number of proteins

for which the up-regulation is not so easily explained through pleiotropic effects, in particular those proteins involved in DNA metabolism and the regulation of plastid gene expression. Therefore, we have shifted efforts to more direct substrate protease interactions, focusing on the putative ClpS substrate regulator (K. Nishimura, Y. Asakura, G. Friso, J. Kim, S.H. Oh, H. Rutschow, L. Ponnala, and K.J. van Wijk, unpublished data).

Why Is the Clp Machinery Needed in the Embryo Plastids and Subsequent Seedling Development?

Solving the question of why the ClpPR protease is needed for embryogenesis requires an understanding of the role of the plastid in the embryo during seed development. During seed development, embryo plastids begin to differentiate into green chloroplasts at the torpedo stage and then become colorless during seed ripening, as chloroplasts dedifferentiate to nonphotosynthetic plastids by losing their thylakoids and associated chlorophylls. Upon germination, these dedifferentiated plastids are converted into chloroplasts in the cotyledons (Ciamporova and Pretova, 1980; for review of the significance and biogenesis of plastids in embryogenesis, see Hsu et al., 2010; Bryant et al., 2011).

In the light of the recent analysis of embryogenesis mutants, it is perhaps surprising that the ClpP4/ClpP5 proteins are required at that very early state of embryogenesis; most genes in this category are metabolic enzymes involved, for example, in the biosynthesis of acetyl-CoA, folate, etc., although others are involved in protein import and plastid gene expression (Hsu et al., 2010). The lack of normal chloroplast development in the seeds of ClpR2, ClpR4, and ClpP3 null mutants apparently results in a developmental block at the cotyledon stage upon germination. Once this block is broken, by the addition of either Glc or Suc to the growth medium, cotyledons unfold and true leaves are formed. These *CLP* alleles do not have white cotyledons, as observed for a subset of plastid mutants, the locus *white cotyledon1* (Yamamoto et al., 2000), the *cyo1* stromal elongation factor G (SCO1; Albrecht et al., 2006; Ruppel and Hangarter, 2007), or the thylakoid protein disulfide isomerase CYO1/SCO2 (Shimada et al., 2007; Albrecht et al., 2008; Tanz et al., 2012; for review, see Pogson and Albrecht, 2011). These *sco* mutants are not affected in chloroplast development during embryogenesis in the developing silique. After initial growth on Suc, these *sco* mutants can be transferred to soil and continue their life cycle under autotrophic conditions, without obvious defects in the chloroplasts of rosette leaves. A different class of mutants have a white-cotyledon phenotype but require sugars to develop green true leaves, such as plastid type I signal peptidase1 (Shipman and Inoue, 2009; Shipman-Roston et al., 2010; Ruppel et al., 2011). Once green leaves have developed, these mutants can grow autotrophically. In contrast, the Clp protease mutants have strong chloroplast phenotypes even when grown under heterotrophic conditions. Thus, the role of the Clp protease system in plant development and plastid function is clearly distinct from the specific developmental program for plastid development in cotyledons. The main challenge now is to determine direct substrates and substrate recognition mechanisms for the Clp system. Based on the collective data set, we hypothesize that proteins involved in DNA metabolism and the regulation of plastid gene expression may represent Clp substrates (e.g. pTAC17). These candidates provide an excellent starting point to study Clp substrate selection.

MATERIALS AND METHODS

Plant Growth, Mutant Isolation, and RT-PCR Analysis

The T-DNA insertion lines in Arabidopsis (*Arabidopsis thaliana*) Columbia-0 for *CLPP3* (AT1G66670) and *CLPP4* (AT5g45390) are SALK_000913 and SALK_065330, respectively. The locations of the T-DNA insertions were confirmed by DNA sequencing. Genotyping and RNA extraction were carried out as described previously (Rudella et al., 2006). Various growth conditions are detailed in the figure legends. For RT-PCR, total RNA was isolated with the RNeasy Plant Mini Kit (Qiagen). The first strand was synthesized from equal amounts of total RNA with SuperScript III Reverse Transcriptase (Invitrogen). We tested 15, 20, 25, and 30 cycles for the primer pairs. Fifteen cycles were insufficient to visualize all transcripts, while 20 and 25 cycles best allowed us to visualize the transcripts, and we observed good linearity for 20 and 25 cycles. Primers for genomic PCR and RT-PCR analysis and various complementations are listed in Supplemental Table S6.

Complementation

Full-length *CLPP4*, *CLPP5*, and *CLPP6* cDNA fragments and a 3,424-bp genomic *CLPP3* DNA fragment were amplified using Taq polymerase. Primers for complementation are also listed in Supplemental Table S6. The PCR products were subcloned into pCR8/GW/TOPO vector (Invitrogen). Using Gateway LR clonase (Invitrogen), the DNA was introduced into pMDC123 (for genomic), pEARLEYGATE100, or pMDC32 (for cDNA) Gateway destination plant binary vector (Curtis and Grossniklaus, 2003). *Agrobacterium tumefaciens* transformation, plant transformation, and selection were carried out as described previously (Rudella et al., 2006).

Microscopy of Developing Seeds

Seeds were removed from siliques and cleared for 1 to 24 h in Hoyer's solution (3.75 g of gum arabic, 50 g of chloral hydrate, and 2.5 mL of glycerol in 15 mL of water) on a microscope slide. Seeds of later developmental stages required extended clearing periods. Cleared seeds were examined using Nomarski optics on an Olympus BX51 microscope.

Plant Growth to Test the Effects of Sugars

To test the sugar effects, the wild type, *clpr2-1*, and *clpp3-1* were grown on one-half-strength Murashige and Skoog agar (0.8% agar) plates with 0%, 1%, 3%, and 5% Suc or Glc under 8-h/16-h light/dark cycles at 40 μmol photons m^{-2} s^{-1}.

Pigment Analysis

Chlorophyll and carotenoid contents on a fresh weight basis were measured in 80% acetone as described (Lichtenthaler, 1987).

Chloroplast Stroma and Total Leaf Proteome Isolation for Analysis of Clp Assembly States

For chloroplast stroma isolation, leaves of the wild type and various mutant alleles were briefly homogenized in grinding medium (50 mM HEPES-KOH,

pH 8.0, 330 mm sorbitol, 2 mM EDTA, 5 mM ascorbic acid, 5 mM Cys, and 0.03% bovine serum albumin) and filtered through a nylon mesh. The crude plastids were then collected by a 2-min spin at 1,100*g* and further purified on 40% to 85% Percoll cushions (Percoll in 0.6% Ficoll and 1.8% polyethylene glycol) by a 10-min spin at 3,750*g* and one additional wash in the grinding medium without ascorbic acid, Cys, and bovine serum albumin. Chloroplasts were subsequently lysed in 10 mM HEPES-KOH, pH 8.0, 5 mM $MgCl_2$, and 15% glycerol with a mixture of protease inhibitors under mild mechanical disruption. The lysate was then subjected to ultracentrifugation (100,000*g*) to pellet the membrane components. The supernatant (stroma) was then collected and concentrated using Amicon 4, 10-kD molecular weight cutoff (Millipore). Protein amounts were determined using the Bradford reagent (Bio-Rad) or the BCA Protein Assay Kit (Thermo Scientific). For total leaf proteome isolation under nondenaturing conditions, total leaf material was ground in liquid nitrogen and solubilized in 50 mM HEPES-KOH, pH 8.0, 15% glycerol, and 10 mM $MgCl_2$ with protease inhibitor cocktail. The suspension was then filtered in Miracloth and spun at 100,000*g*.

Native PAGE Analysis

Light blue native PAGE was performed for the separation of stromal and total leaf extracts under nondenaturing conditions using the NativePAGE Novex gel system (Invitrogen) with precast 4% to 16% acrylamide Bis-Tris gels (Invitrogen).

Immunoblot Analysis

For immunoblots, proteins were blotted onto nitrocellulose or polyvinylidene difluoride membranes and probed with antibodies using chemiluminescence for detection, following standard procedures. Antisera against ClpP3, ClpP4, ClpP6, ClpT1, and ClpT2 were generated in rabbits against protein domains [ClpP3 (Δ1-71), ClpP4 (Δ1-60), ClpP6 (Δ1-51), ClpT1 (Δ1-64), and ClpT2 (Δ1-75)] overexpressed in *Escherichia coli*. Crude antisera were affinity purified using these overexpressed antigens as bait. Additional antisera used were generous gifts from various colleagues: anti-RH3 and anti-OEC23 (from Dr. Alice Barkan), anti-PsaF (from Dr. Hendrik Scheller), anti-Cpn60α (from Dr. Masato Nakai), anti-ClpC2 (from Dr. Steve Rodermel), anti-SppA (from Dr. Anna Sokolenko), and anti-FtsH5 (from Dr. Wataru Sakamoto).

QconCAT Analysis

The design, expression, and purification of the stable isotope-labeled Clp-QconCAT protein used here for MS-based quantification has been described (Olinares et al., 2011a). Prior to SDS-PAGE separation, guanidine was removed from the purified Clp-QconCAT as described (Mirzaei et al., 2008). Equal volumes of 20% TCA and purified Clp-QconCAT were mixed and incubated on ice for 30 min. The acidified solution was then centrifuged at 6,000*g* at 4°C for 15 min, and the supernatant was carefully removed. The pellet was washed twice with 1 mL of 80% cold acetone, vortexed, and centrifuged at 18,000*g* at 4°C for 5 min, and acetone was decanted. The pellet was then dried in a speed vacuum concentrator to fully remove acetone and resuspended with a brief sonication on ice in 50 mM Tris, pH 6.8, and 1% SDS. Protein concentration was determined by the BCA Protein Assay Kit (Thermo Scientific). Samples were then separated on a precast 10.5% to 14% gradient acrylamide Laemmli gel (Bio-Rad), and protein bands were stained with Coomassie dye. Stromal proteomes of the wild type and *clpp3-1* were run out on native PAGE separation, and selected gel regions containing Clp assemblies and SDS-PAGE-separated labeled Clp-QconCAT protein were excised and in-gel digested separately with trypsin. LC-MS analysis and data processing for the absolute quantification of Clp subunits were carried out as described (Olinares et al., 2011a).

Large-Scale Quantitative Proteomics

Wild-type (Columbia-0) plants were grown on soil for 40 d under a short-day cycle (10 h/14 h of light/dark) at 100 μmol photons m^{-2} s^{-1}. Homozygous *clpp3-1* plants were first grown on agar plates with one-half-strength Murashige and Skoog medium and 2% Suc under short-day conditions at 40 μmol photons m^{-2} s^{-1}, then transferred to soil after 70 d and grown under a short-day cycle at 100 μmol photons m^{-2} s^{-1} for another 40 d. Total leaf proteins were extracted by grinding 180 mg of fresh leaves in liquid nitrogen into a fine powder. One milliliter of extraction buffer (1% SDS, 125 mM Tris-HCl [pH 8.8], 5 mM EDTA, 5 mM tributylphosphine, and 2.5 mg mL^{-1} protease inhibitor Pefablok) was added, and a pestle was used to solubilize the material. Unsolubilized materials were removed by centrifugation, and proteins in the resulting supernatant were precipitated in 75% acetone at −80°C. Proteins were collected as pellets by centrifugation, followed by two additional acetone washes to remove lipids. The resulting protein pellet was solubilized in 1% SDS and 50 mM Tris-HCl (pH 8.25), and protein concentrations were determined using the BCA Protein Assay Kit (Thermo Scientific). Fifty micrograms total leaf protein of *clpp3-1* and wild-type samples was run out on Bio-Rad Criterion Tris-HCl precast gels (10.5%–14% acrylamide gradient). Each of the gel lanes were cut into 20 bands followed by reduction, alkylation, and in-gel digestion with trypsin as described (Shevchenko et al., 2006; Friso et al., 2011).

The resuspended peptide extracts were analyzed by data-dependent MS/MS using an online LC-LTQ-Orbitrap (Thermo Scientific). Peptide samples were automatically loaded on a guard column (LC Packings; MGU-30-C18PM) via an autosampler followed by separation on a PepMap C_{18} reverse-phase nanocolumn (LC Packings; nan75-15-03-C18PM) using 90-min gradients with 95% water, 5% acetonitrile, 0.1% formic acid (solvent A) and 95% acetonitrile, 5% water, 0.1% fatty acid (solvent B) at a flow rate of 200 nL min^{-1}. Two blanks were run after every sample (for the gradient and sample injection scheme, see Zybailov et al., 2009b). The acquisition cycle consisted of a survey MS scan in the Orbitrap with a set mass range from 350 to 1,800 mass-to-charge ratio at the highest resolving power (100,000) followed by five data-dependent MS/MS scans acquired in the LTQ. Dynamic exclusion was used with the following parameters: exclusion size, 500; repeat count, two; repeat duration, 30 s; exclusion time, 180 s; exclusion window, ±6 ppm or ±100 ppm. Target values were set at 5×10^5 and 10^4 for the survey and tandem MS scans, respectively. The MS survey scan in the Orbitrap was acquired in one microscan. Fragment ion spectra were acquired in the LTQ as an average of three microscans. MS data processing, data searching against The Arabidopsis Information Resource 8 using Mascot, and subsequent filtering and quantification based on normalized and adjusted spectral counts were carried out as described (Zybailov et al., 2009b) and as outlined in Supplemental Figure S2. MS-derived information, as well as annotation of protein name, location, and function for the identified proteins, can be found in the Plant Proteome Database (http://ppdb.tc.cornell.edu/). The MASIC software (Monroe et al., 2008; http://www.pnl.gov/) was used to extract MS and MS/MS relevant statistics such as duty cycle from Thermo raw files. The files for the 120 LC-MS runs were deposited at the Proteomics Identification Database (http://www.ebi.ac.uk/pride/; Vizcaíno et al., 2013) with accession numbers 16524 to 16643.

Significance Analysis of Large-Scale Spectral Counting-Based Quantification

The GLEE software was developed in MATLAB version 7 (MathWorks), and a stand-alone executable version of the software code using the MATLAB Compiler was created (A. Poliakov, L. Ponnala, P.D. Olinares, and K.J. van Wijk, unpublished data). GLEE was run in a Windows platform with a cubic polynomial equation fitting, adaptive binning, and 20,000 iterations for the estimation of variation. QSpec analysis was performed in a LINUX platform using the software provided from Choi et al. (2008). A total of 5,000 Markov chain Monte Carlo simulations were performed with 20,000 iterations to ensure convergence of the algorithm. No normalization by protein length or peptide length was included.

Assignment of Functional Categories

Protein functions were assigned using the MapMan bin system (Thimm et al., 2004) that we further curated and incorporated into the Plant Proteome Database at http://ppdb.tc.cornell.edu.

Proteomics data are available via the Proteomics Identifications database under accession numbers 16524 to 16632 and via the Plant Proteome database.

Supplemental Data

The following materials are available in the online version of this article.

Supplemental Figure S1. Effects of Suc and Glc in the wild type, *clpr2-1*, and *clpp3-1* on pigment levels measured after 28 d of sowing.

Supplemental Figure S2. MS analysis and bioinformatics workflow for the comparative proteome analysis.

Supplemental Figure S3. Comparison of LTQ-Orbitrap data acquisition cycles in comparative proteomics studies of *clpr2* (Zybailov et al., 2009a), *clpr4* (Kim et al., 2009), and *clpp3* (this study) mutants.

Supplemental Table S1. Chlorophyll and carotenoid accumulation in *clpp3-1* grown on agar (2% Suc) or soil.

Supplemental Table S2. Quantification of Clp subunits and determination of subunit stoichiometry in various Clp assemblies in the wild type and *clpp3-1* using the QConCAT technique.

Supplemental Table S3. Large-scale comparative proteomics of the *clpp3-1* mutant and the wild type.

Supplemental Table S4. Summary of the subcellular locations and investment in *clpp3-1* and wild-type proteins.

Supplemental Table S5. Sample preparation, MS data acquisition parameters, peptide match rates, and identified proteins among the Clp comparative proteomic studies.

Supplemental Table S6. Primers used for genotyping, RT-PCR, and complementation.

Supplemental Text S1. Technical comparison of the current *clpp3-1* analysis with comparative proteomics studies of Clp mutants and comment on the development of the GLEE statistical package.

ACKNOWLEDGMENTS

We thank Yukari Asakura for generation of the anti-ClpR2 and anti-ClpS antisera. We thank Verenice Ramirez Rodriquez for genomic complementation of *clpp3-1*. We thank Dr. Qi Sun for his valuable support with the Plant Proteome Database and other bioinformatics-related aspects. We acknowledge Drs. Alice Barkan, Hendrik Scheller, Masato Nakai, Steve Rodermel, Anna Sokolenko, Wataru Sakamoto, and Zach Adam for providing antisera for the immunoblot analyses. We also thank Dr. Wojtek Pawlowski and Dr. Arnaud Ronceret for use of the Nomarski optics microscope and for providing valuable help.

Received February 4, 2013; accepted March 27, 2013; published April 2, 2013.

LITERATURE CITED

Albrecht V, Ingenfeld A, Apel K (2006) Characterization of the snowy cotyledon 1 mutant of Arabidopsis thaliana: the impact of chloroplast elongation factor G on chloroplast development and plant vitality. Plant Mol Biol **60:** 507–518

Albrecht V, Ingenfeld A, Apel K (2008) Snowy cotyledon 2: the identification of a zinc finger domain protein essential for chloroplast development in cotyledons but not in true leaves. Plant Mol Biol **66:** 599–608

Asakura Y, Galarneau ER, Watkins KP, Barkan A, van Wijk KJ (2012) Chloroplast RH3 DEAD box RNA helicases in maize and Arabidopsis function in splicing of specific group II introns and affect chloroplast ribosome biogenesis. Plant Physiol **159:** 961–974

Beynon RJ, Doherty MK, Pratt JM, Gaskell SJ (2005) Multiplexed absolute quantification in proteomics using artificial QCAT proteins of concatenated signature peptides. Nat Methods **2:** 587–589

Bhushan S, Ståhl A, Nilsson S, Lefebvre B, Seki M, Roth C, McWilliam D, Wright SJ, Liberles DA, Shinozaki K, et al (2005) Catalysis, subcellular localization, expression and evolution of the targeting peptides degrading protease, AtPreP2. Plant Cell Physiol **46:** 985–996

Boston RS, Viitanen PV, Vierling E (1996) Molecular chaperones and protein folding in plants. Plant Mol Biol **32:** 191–222

Bréhélin C, Kessler F, van Wijk KJ (2007) Plastoglobules: versatile lipoprotein particles in plastids. Trends Plant Sci **12:** 260–266

Britton RA, Wen TY, Schaefer L, Pellegrini O, Uicker WC, Mathy N, Tobin C, Daou R, Szyk J, Condon C (2007) Maturation of the 5′ end of Bacillus subtilis 16S rRNA by the essential ribonuclease YkqC/RNase J1. Mol Microbiol **63:** 127–138

Bryant N, Lloyd J, Sweeney C, Myouga F, Meinke D (2011) Identification of nuclear genes encoding chloroplast-localized proteins required for embryo development in Arabidopsis. Plant Physiol **155:** 1678–1689

Cappadocia L, Parent JS, Zampini E, Lepage E, Sygusch J, Brisson N (2012) A conserved lysine residue of plant Whirly proteins is necessary for higher order protein assembly and protection against DNA damage. Nucleic Acids Res **40:** 258–269

Chen G, Bi YR, Li N (2005) EGY1 encodes a membrane-associated and ATP-independent metalloprotease that is required for chloroplast development. Plant J **41:** 364–375

Chen G, Law K, Ho P, Zhang X, Li N (2012) EGY2, a chloroplast membrane metalloprotease, plays a role in hypocotyl elongation in Arabidopsis. Mol Biol Rep **39:** 2147–2155

Choi H, Fermin D, Nesvizhskii AI (2008) Significance analysis of spectral count data in label-free shotgun proteomics. Mol Cell Proteomics **7:** 2373–2385

Ciamporova M, Pretova A (1980) Ultrastructural changes of plastids in flax embryos cultivated in vitro. New Phytol **87:** 473–479

Curtis MD, Grossniklaus U (2003) A Gateway cloning vector set for high-throughput functional analysis of genes in planta. Plant Physiol **133:** 462–469

Derrien B, Majeran W, Effantin G, Ebenezer J, Friso G, van Wijk KJ, Steven AC, Maurizi MR, Vallon O (2012) The purification of the Chlamydomonas reinhardtii chloroplast ClpP complex: additional subunits and structural features. Plant Mol Biol **80:** 189–202

Eveland AL, Jackson DP (2012) Sugars, signalling, and plant development. J Exp Bot **63:** 3367–3377

Ferbitz L, Maier T, Patzelt H, Bukau B, Deuerling E, Ban N (2004) Trigger factor in complex with the ribosome forms a molecular cradle for nascent proteins. Nature **431:** 590–596

Friso G, Olinares PDB, van Wijk KJ (2011) The workflow for quantitative proteome analysis of chloroplast development and differentiation, chloroplast mutants, and protein interactions by spectral counting. *In* RP Jarvis, ed, Chloroplast Research in Arabidopsis, Vol 775. Humana Press, New York, pp 265–282

Ganeteg U, Klimmek F, Jansson S (2004) Lhca5: an LHC-type protein associated with photosystem I. Plant Mol Biol **54:** 641–651

Glaser E, Nilsson S, Bhushan S (2006) Two novel mitochondrial and chloroplastic targeting-peptide-degrading peptidasomes in A. thaliana, AtPreP1 and AtPreP2. Biol Chem **387:** 1441–1447

Goloubinoff P, Mogk A, Zvi AP, Tomoyasu T, Bukau B (1999) Sequential mechanism of solubilization and refolding of stable protein aggregates by a bichaperone network. Proc Natl Acad Sci USA **96:** 13732–13737

Hanson J, Smeekens S (2009) Sugar perception and signaling: an update. Curr Opin Plant Biol **12:** 562–567

Haslberger T, Zdanowicz A, Brand I, Kirstein J, Turgay K, Mogk A, Bukau B (2008) Protein disaggregation by the AAA+ chaperone ClpB involves partial threading of looped polypeptide segments. Nat Struct Mol Biol **15:** 641–650

Hein P, Stöckel J, Bennewitz S, Oelmüller R (2009) A protein related to prokaryotic UMP kinases is involved in psaA/B transcript accumulation in Arabidopsis. Plant Mol Biol **69:** 517–528

Hsu SC, Belmonte MF, Harada JJ, Inoue K (2010) Indispensable roles of plastids in Arabidopsis thaliana embryogenesis. Curr Genomics **11:** 338–349

Huang M, Friso G, Nishimura K, Qu X, Olinares PD, Majeran W, Sun Q, van Wijk KJ (2013) Construction of plastid reference proteomes for maize and Arabidopsis and evaluation of their orthologous relationships: the concept of orthoproteomics. J Proteome Res **12:** 491–504

Kabeya Y, Nakanishi H, Suzuki K, Ichikawa T, Kondou Y, Matsui M, Miyagishima SY (2010) The YlmG protein has a conserved function related to the distribution of nucleoids in chloroplasts and cyanobacteria. BMC Plant Biol **10:** 57

Kato Y, Sakamoto W (2010) New insights into the types and function of proteases in plastids. Int Rev Cell Mol Biol **280:** 185–218

Kato Y, Sun X, Zhang L, Sakamoto W (2012) Cooperative D1 degradation in the photosystem II repair mediated by chloroplastic proteases in Arabidopsis. Plant Physiol **159:** 1428–1439

Kessler F, Schnell DJ (2006) The function and diversity of plastid protein import pathways: a multilane GTPase highway into plastids. Traffic **7:** 248–257

Kim J, Rudella A, Ramirez Rodriguez V, Zybailov B, Olinares PD, van Wijk KJ (2009) Subunits of the plastid ClpPR protease complex have differential contributions to embryogenesis, plastid biogenesis, and plant development in *Arabidopsis*. Plant Cell **21:** 1669–1692

Koussevitzky S, Stanne TM, Peto CA, Giap T, Sjögren LL, Zhao Y, Clarke AK, Chory J (2007) An Arabidopsis thaliana virescent mutant reveals a role for ClpR1 in plastid development. Plant Mol Biol **63:** 85–96

Krause K, Kilbienski I, Mulisch M, Rödiger A, Schäfer A, Krupinska K (2005) DNA-binding proteins of the Whirly family in Arabidopsis thaliana are targeted to the organelles. FEBS Lett **579:** 3707–3712

Kuroda H, Maliga P (2003) The plastid clpP1 protease gene is essential for plant development. Nature **425:** 86–89

Lensch M, Herrmann RG, Sokolenko A (2001) Identification and characterization of SppA, a novel light-inducible chloroplast protease complex associated with thylakoid membranes. J Biol Chem **276:** 33645–33651

Lichtenthaler HK (1987) Chlorophylls and carotenoids: pigments of photosynthetic biomembranes. Methods Enzymol **148:** 350–382

Lippuner V, Chou IT, Scott SV, Ettinger WF, Theg SM, Gasser CS (1994) Cloning and characterization of chloroplast and cytosolic forms of cyclophilin from Arabidopsis thaliana. J Biol Chem **269:** 7863–7868

Liu X, Yu F, Rodermel S (2010a) An Arabidopsis pentatricopeptide repeat protein, SUPPRESSOR OF VARIEGATION7, is required for FtsH-mediated chloroplast biogenesis. Plant Physiol **154:** 1588–1601

Liu X, Yu F, Rodermel S (2010b) Arabidopsis chloroplast FtsH, var2 and suppressors of var2 leaf variegation: a review. J Integr Plant Biol **52:** 750–761

Lucinski R, Schmid VH, Jansson S, Klimmek F (2006) Lhca5 interaction with plant photosystem I. FEBS Lett **580:** 6485–6488

Lundquist P, Poliakov A, Bhuiyan NH, Zybailov B, Sun Q, van Wijk KJ (2012) The functional network of the Arabidopsis plastoglobule proteome based on quantitative proteomics and genome-wide co-expression analysis. Plant Physiol **58:** 1172–1192

Majeran W, Friso G, Asakura Y, Qu X, Huang M, Ponnala L, Watkins KP, Barkan A, van Wijk KJ (2012) Nucleoid-enriched proteomes in developing plastids and chloroplasts from maize leaves: a new conceptual framework for nucleoid functions. Plant Physiol **158:** 156–189

Maréchal A, Parent JS, Véronneau-Lafortune F, Joyeux A, Lang BF, Brisson N (2009) Whirly proteins maintain plastid genome stability in Arabidopsis. Proc Natl Acad Sci USA **106:** 14693–14698

Meinke D, Sweeney C, Muralla R (2009) Integrating the genetic and physical maps of Arabidopsis thaliana: identification of mapped alleles of cloned essential (EMB) genes. PLoS ONE **4:** e7386

Mirzaei H, McBee JK, Watts J, Aebersold R (2008) Comparative evaluation of current peptide production platforms used in absolute quantification in proteomics. Mol Cell Proteomics **7:** 813–823

Monroe ME, Shaw JL, Daly DS, Adkins JN, Smith RD (2008) MASIC: a software program for fast quantitation and flexible visualization of chromatographic profiles from detected LC-MS(/MS) features. Comput Biol Chem **32:** 215–217

Munshi MK, Kobayashi Y, Shikanai T (2006) Chlororespiratory reduction 6 is a novel factor required for accumulation of the chloroplast NAD(P)H dehydrogenase complex in Arabidopsis. Plant Physiol **141:** 737–744

Myouga F, Motohashi R, Kuromori T, Nagata N, Shinozaki K (2006) An Arabidopsis chloroplast-targeted Hsp101 homologue, APG6, has an essential role in chloroplast development as well as heat-stress response. Plant J **48:** 249–260

Olinares PD, Kim J, Davis JI, van Wijk KJ (2011a) Subunit stoichiometry, evolution, and functional implications of an asymmetric plant plastid ClpP/R protease complex in *Arabidopsis*. Plant Cell **23:** 2348–2361

Olinares PD, Kim J, van Wijk KJ (2011b) The Clp protease system: a central component of the chloroplast protease network. Biochim Biophys Acta **1807:** 999–1011

Peltier JB, Cai Y, Sun Q, Zabrouskov V, Giacomelli L, Rudella A, Ytterberg AJ, Rutschow H, van Wijk KJ (2006) The oligomeric stromal proteome of Arabidopsis thaliana chloroplasts. Mol Cell Proteomics **5:** 114–133

Peltier JB, Ripoll DR, Friso G, Rudella A, Cai Y, Ytterberg J, Giacomelli L, Pillardy J, van Wijk KJ (2004) Clp protease complexes from photosynthetic and non-photosynthetic plastids and mitochondria of plants, their predicted three-dimensional structures, and functional implications. J Biol Chem **279:** 4768–4781

Peng L, Cai W, Shikanai T (2010) Chloroplast stromal proteins, CRR6 and CRR7, are required for assembly of the NAD(P)H dehydrogenase subcomplex A in Arabidopsis. Plant J **63:** 203–211

Pfalz J, Liere K, Kandlbinder A, Dietz KJ, Oelmüller R (2006) pTAC2, -6, and -12 are components of the transcriptionally active plastid chromosome that are required for plastid gene expression. Plant Cell **18:** 176–197

Pogson BJ, Albrecht V (2011) Genetic dissection of chloroplast biogenesis and development: an overview. Plant Physiol **155:** 1545–1551

Pratt JM, Simpson DM, Doherty MK, Rivers J, Gaskell SJ, Beynon RJ (2006) Multiplexed absolute quantification for proteomics using concatenated signature peptides encoded by QconCAT genes. Nat Protoc **1:** 1029–1043

Prikryl J, Watkins KP, Friso G, van Wijk KJ, Barkan A (2008) A member of the Whirly family is a multifunctional RNA- and DNA-binding protein that is essential for chloroplast biogenesis. Nucleic Acids Res **36:** 5152–5165

Reinhold T, Alawady A, Grimm B, Beran KC, Jahns P, Conrath U, Bauer J, Reiser J, Melzer M, Jeblick W, et al (2007) Limitation of nocturnal import of ATP into Arabidopsis chloroplasts leads to photooxidative damage. Plant J **50:** 293–304

Richter S, Lamppa GK (1998) A chloroplast processing enzyme functions as the general stromal processing peptidase. Proc Natl Acad Sci USA **95:** 7463–7468

Richter S, Lamppa GK (1999) Stromal processing peptidase binds transit peptides and initiates their ATP-dependent turnover in chloroplasts. J Cell Biol **147:** 33–44

Rudella A, Friso G, Alonso JM, Ecker JR, van Wijk KJ (2006) Downregulation of ClpR2 leads to reduced accumulation of the ClpPRS protease complex and defects in chloroplast biogenesis in *Arabidopsis*. Plant Cell **18:** 1704–1721

Ruppel NJ, Hangarter RP (2007) Mutations in a plastid-localized elongation factor G alter early stages of plastid development in Arabidopsis thaliana. BMC Plant Biol **7:** 37

Ruppel NJ, Logsdon CA, Whippo CW, Inoue K, Hangarter RP (2011) A mutation in Arabidopsis *SEEDLING PLASTID DEVELOPMENT1* affects plastid differentiation in embryo-derived tissues during seedling growth. Plant Physiol **155:** 342–353

Scranton MA, Yee A, Park SY, Walling LL (2012) Plant leucine aminopeptidases moonlight as molecular chaperones to alleviate stress-induced damage. J Biol Chem **287:** 18408–18417

Shevchenko A, Tomas H, Havlis J, Olsen JV, Mann M (2006) In-gel digestion for mass spectrometric characterization of proteins and proteomes. Nat Protoc **1:** 2856–2860

Shikanai T, Shimizu K, Ueda K, Nishimura Y, Kuroiwa T, Hashimoto T (2001) The chloroplast clpP gene, encoding a proteolytic subunit of ATP-dependent protease, is indispensable for chloroplast development in tobacco. Plant Cell Physiol **42:** 264–273

Shimada H, Mochizuki M, Ogura K, Froehlich JE, Osteryoung KW, Shirano Y, Shibata D, Masuda S, Mori K, Takamiya K (2007) *Arabidopsis* cotyledon-specific chloroplast biogenesis factor CYO1 is a protein disulfide isomerase. Plant Cell **19:** 3157–3169

Shipman RL, Inoue K (2009) Suborganellar localization of plastidic type I signal peptidase 1 depends on chloroplast development. FEBS Lett **583:** 938–942

Shipman-Roston RL, Ruppel NJ, Damoc C, Phinney BS, Inoue K (2010) The significance of protein maturation by plastidic type I signal peptidase 1 for thylakoid development in Arabidopsis chloroplasts. Plant Physiol **152:** 1297–1308

Singh DK, McNellis TW (2011) Fibrillin protein function: the tip of the iceberg? Trends Plant Sci **16:** 432–441

Sjögren LL, Clarke AK (2011) Assembly of the chloroplast ATP-dependent Clp protease in *Arabidopsis* is regulated by the ClpT accessory proteins. Plant Cell **23:** 322–332

Sjögren LL, Stanne TM, Zheng B, Sutinen S, Clarke AK (2006) Structural and functional insights into the chloroplast ATP-dependent Clp protease in *Arabidopsis*. Plant Cell **18:** 2635–2649

Ståhl A, Nilsson S, Lundberg P, Bhushan S, Biverståhl H, Moberg P, Morisset M, Vener A, Mäler L, Langel U, et al (2005) Two novel targeting peptide degrading proteases, PrePs, in mitochondria and chloroplasts, so similar and still different. J Mol Biol **349:** 847–860

Stanne TM, Sjögren LL, Koussevitzky S, Clarke AK (2009) Identification of new protein substrates for the chloroplast ATP-dependent Clp protease supports its constitutive role in Arabidopsis. Biochem J **417:** 257–268

Tanz SK, Kilian J, Johnsson C, Apel K, Small I, Harter K, Wanke D, Pogson B, Albrecht V (2012) The SCO2 protein disulphide isomerase is required for thylakoid biogenesis and interacts with LHCB1 chlorophyll a/b binding proteins which affects chlorophyll biosynthesis in Arabidopsis seedlings. Plant J **69:** 743–754

Thimm O, Bläsing O, Gibon Y, Nagel A, Meyer S, Krüger P, Selbig J, Müller LA, Rhee SY, Stitt M (2004) MAPMAN: a user-driven tool to display genomics data sets onto diagrams of metabolic pathways and other biological processes. Plant J **37:** 914–939

Vizcaíno JA, Côté RG, Csordas A, Dianes JA, Fabregat A, Foster JM, Griss J, Alpi E, Birim M, Contell J, et al (2013) The PRoteomics IDEntifications

(PRIDE) database and associated tools: status in 2013. Nucleic Acids Res **41:** D1063–D1069

Walling LL (2006) Recycling or regulation? The role of amino-terminal modifying enzymes. Curr Opin Plant Biol **9:** 227–233

Wandinger SK, Richter K, Buchner J (2008) The Hsp90 chaperone machinery. J Biol Chem **283:** 18473–18477

Xiao Y, Savchenko T, Baidoo EE, Chehab WE, Hayden DM, Tolstikov V, Corwin JA, Kliebenstein DJ, Keasling JD, Dehesh K (2012) Retrograde signaling by the plastidial metabolite MEcPP regulates expression of nuclear stress-response genes. Cell **149:** 1525–1535

Yamamoto YY, Puente P, Deng XW (2000) An Arabidopsis cotyledon-specific albino locus: a possible role in 16S rRNA maturation. Plant Cell Physiol **41:** 68–76

Ytterberg AJ, Peltier JB, van Wijk KJ (2006) Protein profiling of plastoglobules in chloroplasts and chromoplasts: a surprising site for differential accumulation of metabolic enzymes. Plant Physiol **140:** 984–997

Zheng B, MacDonald TM, Sutinen S, Hurry V, Clarke AK (2006) A nuclear-encoded ClpP subunit of the chloroplast ATP-dependent Clp protease is essential for early development in Arabidopsis thaliana. Planta **224:** 1103–1115

Zybailov B, Friso G, Kim J, Rudella A, Rodríguez VR, Asakura Y, Sun Q, van Wijk KJ (2009a) Large scale comparative proteomics of a chloroplast Clp protease mutant reveals folding stress, altered protein homeostasis, and feedback regulation of metabolism. Mol Cell Proteomics **8:** 1789–1810

Zybailov B, Rutschow H, Friso G, Rudella A, Emanuelsson O, Sun Q, van Wijk KJ (2008) Sorting signals, N-terminal modifications and abundance of the chloroplast proteome. PLoS ONE **3:** e1994

Zybailov B, Sun Q, van Wijk KJ (2009b) Workflow for large scale detection and validation of peptide modifications by RPLC-LTQ-Orbitrap: application to the Arabidopsis thaliana leaf proteome and an online modified peptide library. Anal Chem **81:** 8015–8024